Science of the Total Environment 658 (2019) 1316–1333

Contents lists available at ScienceDirect

Science of the Total Environment

journal homepage: www.elsevier.com/locate/scitotenv

Investigation of ozone deposition to vegetation under warm and dry conditions near the Eastern Mediterranean coast

Qian Li [a], Maor Gabay [a], Yoav Rubin [a], Shira Raveh-Rubin [b], Shani Rohatyn [b], Fyodor Tatarinov [b], Eyal Rotenberg [b], Efrat Ramati [b], Uri Dicken [b], Yakir Preisler [b], Erick Fredj [c], Dan Yakir [b], Eran Tas [a,*]

[a] The Robert H. Smith Faculty of Agriculture, Food and Environment, Department of Soil and Water Sciences, The Hebrew University of Jerusalem, Rehovot, Israel
[b] Earth and Planetary Sciences, Weizmann Institute of Science, Rehovot, Israel
[c] Department of Computer Science, Jerusalem College of Technology, Jerusalem, Israel

HIGHLIGHTS

- Semiarid drought conditions strongly reduce O_3 flux from spring to late autumn.
- Small stomatal O_3 fraction was indicated for O_3 deposition to semiarid forest.
- Extreme dry surface events can result in positive O_3 flux from a forest.
- Sea and land breeze can significantly enhance nighttime O_3 deposition to vegetation.
- Relative humidity is a major factor in O_3 deposition under the studied conditions.

GRAPHICAL ABSTRACT

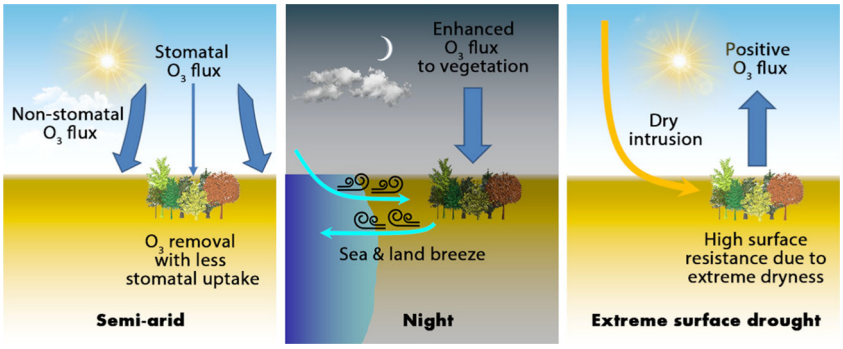

ARTICLE INFO

Article history:
Received 26 October 2018
Received in revised form 17 December 2018
Accepted 18 December 2018
Available online 19 December 2018

Editor: Elena Paoletti

Keywords:
Eddy covariance
Semiarid
Relative humidity
Dry intrusion
Sea/land breeze

ABSTRACT

Dry deposition of ozone (O_3) to vegetation is an important removal pathway for tropospheric O_3, while O_3 uptake through plant stomata negatively affects vegetation and leads to climate change. Both processes are controlled by vegetation characteristics and ambient conditions via complex mechanisms. Recent studies have revealed that these processes can be fundamentally impacted by coastal effects, and by dry and warm conditions in ways that have not been fully characterized, largely due to lack of measurements under such conditions. Hence, we hypothesized that measuring dry deposition of O_3 to vegetation along a sharp spatial climate gradient, and at different distances from the coast, can offer new insights into the characterization of these effects on O_3 deposition to vegetation and stomatal uptake, providing important information for afforestation management and for climate and air-quality model improvement. To address these hypotheses, several measurement campaigns were performed at different sites, including pine, oak, and mixed Mediterranean forests, at distances of 20–59 km from the Eastern Mediterranean coast, under semiarid, Mediterranean and humid Mediterranean climate conditions. The eddy covariance technique was used to quantify vertical O_3 flux (F_{tot}) and its partitioning to stomatal flux (F_{st}) and non-stomatal flux (F_{ns}). Whereas F_{st} tended to peak around noon under humid Mediterranean and Mediterranean conditions in summer, it was strongly limited by drought under semiarid conditions from spring to early winter, with minimum average F_{st}/F_{tot} of 8–11% during the summer. F_{ns} in the area was predominantly controlled by relative humidity (RH), whereas increasing F_{ns} with RH for RH < 70% indicated enhancement of F_{ns} by aerosols, via surface wetness stimulation. At night, efficient turbulence due to sea and land breezes, together

* Corresponding author at: The Department of Soil and Water Sciences, The Robert H. Smith Faculty of Agriculture, Food and Environment, Hebrew University of Jerusalem, Rehovot, Israel.
E-mail address: eran.tas@mail.huji.ac.il (E. Tas).

https://doi.org/10.1016/j.scitotenv.2018.12.272

with increased RH, resulted in strong enhancement of F_{tot}. Extreme dry surface events, some induced by dry intrusion from the upper troposphere, resulted in positive F_{ns} events.

1. Introduction

Dry deposition is an important removal process of ozone (O_3), a phytotoxic air pollutant and greenhouse gas which also plays a key role in the oxidation capacity of the atmosphere (Finlayson-Pitts and Pitts, 2000; Kley et al., 1999; WHO, 2006). While dry deposition is estimated to account for about 20–25% of total O_3 removal from the troposphere (Lelieveld and Dentener, 2000; Wild, 2007), O_3 deposition rate to vegetation tends to be higher than to non-vegetated surface (Wesely and Hicks, 2000). Deposition of O_3 to vegetation is also important due to uptake of O_3 through plant stomata, which has been shown to cause considerable damage to natural and cultivated plants associated with a reduction in primary production (Ashmore, 2005; Bender and Weigel, 2011; Fiscuc et al., 2005; Fowler et al., 2009; Kley et al., 1999; P. Li et al., 2018; van Dingenen et al., 2009), and to negatively affect climate through changes in transpiration and reduced carbon allocation (Fares et al., 2013; Lombardozzi et al., 2013, 2015; Sitch et al., 2007; Wittig et al., 2007).

O_3 deposition is not well represented by global or regional models, limiting our ability to assess the effects of O_3 on climate and air quality, as well as on vegetation (Ganzeveld et al., 2010; Hardacre et al., 2015; Silva and Heald, 2018; Sun et al., 2012; Wolfe et al., 2011). Using the global GEOS-Chem model, Silva and Heald (2018) revealed a typical bias in calculated deposition velocity of 40%, associated with a local bias in O_3 concentration of up to 4 ppbv and with high sensitivity to land class. Recent studies have clearly indicated that field measurements of O_3 deposition can significantly improve our ability to more accurately represent the O_3 dry deposition to vegetation by models (Hardacre et al., 2015; Rydsaa et al., 2016; Silva and Heald, 2018). Moreover, simulation of stomatal flux of O_3 in models can be improved by more adequately accounting for measurable information on the vegetation, soil and air properties (Anav et al., 2018a; Ashmore, 2005; Emberson et al., 2000; Rydsaa et al., 2016; Val Martin et al., 2014). For instance, inaccurate representation of phenological stage by models has been shown to result in an up to 25% bias in the simulated stomatal O_3 uptake in forests (Anav et al., 2018a), and a generally high bias in simulated surface O_3 concentrations (Val Martin et al., 2014).

Field measurements, in turn, indicate that both stomatal and non-stomatal O_3 fluxes (F_{st} and F_{ns}, respectively), and the partitioning between these components are controlled by complex mechanisms and feedback, and their responses to changing ambient conditions have not been fully characterized. Non-stomatal uptake can be subdivided into gas-phase chemical reactions and surface uptake (Cape et al., 2009; Fowler et al., 2009), while each of the stomatal, surface and gas-phase chemical O_3-loss pathways further depend on air, soil and vegetation properties in a complex manner (e.g., Fares et al., 2010b; Launiainen et al., 2013; Niinemets et al., 2004). This complexity in the response of O_3 deposition mechanisms to changing environmental conditions may be a major reason for inconsistent interpretation of the importance of different pathways controlling O_3 deposition to vegetation, as in the case of the relative importance of gas-phase chemistry vs. surface loss (Wolfe et al., 2011).

O_3 deposition to vegetation and its partitioning to stomatal and non-stomatal components under warm and dry conditions have been shown to differ significantly compared to more temperate conditions (Cieslik, 2009; Emberson et al., 2000; Fowler et al., 2009). Under Mediterranean conditions, F_{st} tends to be highly limited by stomatal conductance due to the high temperature and drought conditions. As a result, the F_{ns} occasionally ranges from 30 to 80% in the Western Mediterranean and California (Cieslik, 2009; Gerosa et al., 2005; Goldstein et al., 2004; Kurpius and Goldstein, 2003). Recently, Q. Li et al. (2018) found an even lower fraction of F_{st} over natural Eastern Mediterranean mixed shrubbery, with average F_{st} out of total O_3 flux (F_{tot}) ranging from ~9 to 24% in the summer to a maximum of <60% in winter. Moreover, while previous studies have indicated significantly higher F_{tot} during the summer vs. winter under Mediterranean and temperate conditions (e.g., Bauer et al., 2000; Gerosa et al., 2009; Kurpius and Goldstein, 2003; Michou et al., 2005), the strong limitation on F_{st} under Eastern Mediterranean conditions in the summer results in a significant decrease in F_{tot} when shifting from winter to summer (Q. Li et al., 2018).

These findings demonstrate that O_3 uptake by vegetation under extremely warm and dry conditions can fundamentally differ, even from most of the Mediterranean regions. Our knowledge of O_3 deposition to natural vegetation under these conditions is very limited, even though a relatively large fraction of global land is located under such conditions. For instance, whereas semiarid areas occupy ~18% of the global land area (Lal, 2004), to the best of our knowledge, no information is currently available on O_3 deposition to semiarid vegetation. Moreover, understanding the feedback of vegetation under extremely warm and dry conditions is important in the context of currently increasing desertification (Becerril-Piña et al., 2015) and afforestation.

In particular, improving our knowledge of the partitioning of F_{tot} to F_{ns} under such conditions is highly important considering that a higher F_{st} fraction can lead to an increase in radiative forcing and negative effects on vegetation, but on the other hand, higher F_{ns} is an important pathway for O_3 removal with no such negative implications (see Ainsworth et al., 2012 and references therein).

Here we apply the eddy covariance (EC) technique to study O_3 deposition to a semiarid pine forest. To the best of our knowledge, this is the first time that O_3 deposition to a semiarid forest has been studied. We further compare the stomatal and non-stomatal flux components with corresponding values of natural vegetation along the Israeli climate gradient (ICG), under Mediterranean and humid Mediterranean climate conditions. Q. Li et al. (2018) also indicated significant stimulation of daytime and nighttime O_3 deposition by coastal effects. The fact that all investigated sites are located 20–59 km from the Eastern Mediterranean coastline is further used to investigate coastal effects on daytime and nighttime O_3 deposition, which have been recently found to be important (Q. Li et al., 2018).

Our main hypotheses were: (i) partitioning of O_3 deposition to vegetation into stomatal and non-stomatal flux can differ significantly under semiarid conditions vs. less extreme dry and warm conditions, such as in Mediterranean areas; (ii) improving our knowledge of O_3 deposition to natural vegetation under extremely dry and warm conditions, and under coastal effects, is crucial for improving climate and air-quality models. We further believe that providing information on total O_3 removal and the fraction that is taken up by vegetation under the studied conditions is important for afforestation management.

2. Methodology

2.1. Measurement sites

Field measurements were carried out at five measurement sites with different vegetation in Israel, 20–59 km from the Eastern Mediterranean coast (see Fig. 1 and Table 1). The sites were selected according to the EC

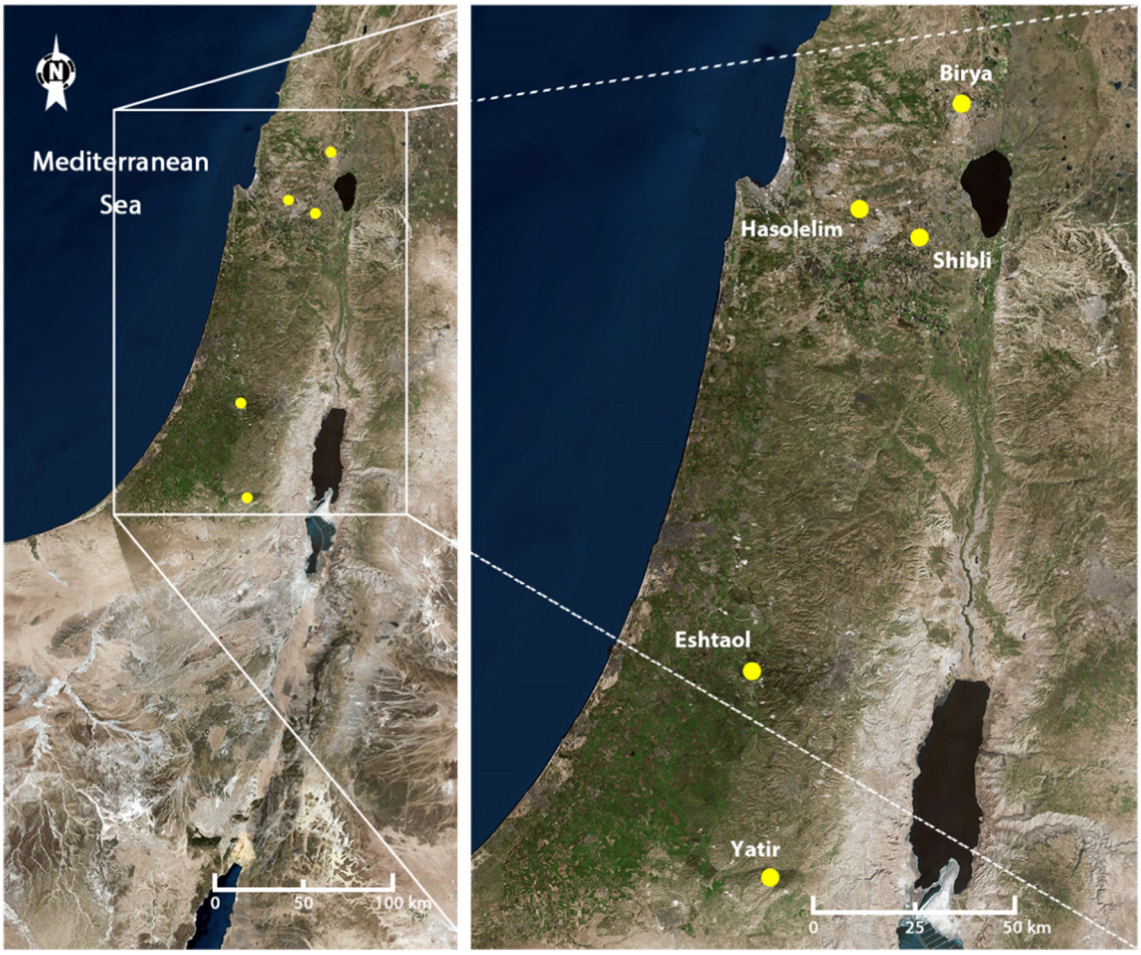

Fig. 1. Location and satellite image of the five measurement sites. The left panel shows the locations of the sites on a large-scale map. The right panel zooms in to show the names of each site.

requirement of a flat, homogeneous surface and their distribution along the ICG. The ICG is characterized by a general decrease in precipitation amount and increased dryness from humid Mediterranean in northern Israel, to semiarid and arid in southern Israel, along with generally high daily temperatures, as described in the following and in Table 1. Three of the sites, Yatir forest (Yat), Eshtaol forest (Esh) and Birya forest (Bir), are predominantly covered by planted pine forest, but exposed to semiarid, Mediterranean and humid Mediterranean climate, respectively (see Table 1), whereas the other two sites, Beit Keshet (Shibli) forest (Shi) and HaSolelim forest (Has), are predominantly covered by mixed-Mediterranean vegetation and oak, and exposed to a Mediterranean climate.

The Yat site, located on a semiarid plateau in the northern Negev, is a 28-km^2 planted forest covered by *Pinus halepensis*, with an understory of mainly *Sarcopoterium spinosum* L., *Phagnalon rupestre* (L.) DC, and a variety of ephemeral herbaceous species. The Bir site, in the Galilee region of northern Israel, is a planted 21-km^2 forest dominated by *Pinus halepensis*, with an understory of mainly *Sarcopoterium spinosum* L. and *Phagnalon rupestre* (L.) DC, and a variety of ephemeral herbaceous species. The Has site, 30 km south of the Bir site, is a native mixed oak forest with an area of 2.4 km^2, predominantly covered by *Quercus ithaburensis*, accompanied by *Quercus calliprinos* (evergreen) and a few other Mediterranean broadleaved tree and shrub species. The Esh site is ca. 12 km^2 of planted pine forest in the central part of Israel,

Table 1
Measurement site characteristics.

Site	Birya	HaSolelim	Shibli	Eshtaol	Yatir
Coordinates	33°00′00.50″N 35°30′40.50″E	32°44′41.41″N 35°13′52.84″E	32°42′16.67″N 35°23′12.18″E	31°47′34.50″N 35°00′11.50″E	31°20′49.20″N 35°03′07.20″E
Climate type	Humid Mediterranean	Mediterranean	Mediterranean	Mediterranean	Semiarid
Annual precipitation	730 mm	562 mm	486 mm	543 mm	285 mm
Mean daily maximum temperature	21.7 °C	27.5 °C	27.4 °C	23.7 °C	24.8 °C
Mean daily minimum temperature	13.1 °C	15.3 °C	15.0 °C	13.4 °C	13.1 °C
Altitude (above sea level)	755 m	180 m	202 m	380 m	650 m
Forest type	Pine forest [PF]	Oak forest [OF]	Mixed Mediterranean forest [MMF]	Pine forest [PF]	Pine forest [PF]
Canopy height	11 m	8 m	5 m	11 m	10 m
Soil type	Rendzina and Terra rossa	Rendzina and Terra rossa	Terra rossa	Light brown Rendzina	Light brown Rendzina

dominated by *Pinus halepensis*. The Shi site, approximately 1200 m × 900 m of homogeneous gentle slope, is located in a ca. 1000-ha forest covered by ~25% *Quercus calliprinos*, 25% *Quercus ithaburensis*, ~20% *Pistacia terebinthus*, ~15% *Pistacia lentiscus*, ~10% *Pinus halepensis* and 5% *Pinus pinea*.

2.2. Field measurements

The field measurements at the five different sites were performed from July 2013 to November 2016. All measured data were classified into 14 different periods (Table 2) according to season, or into shorter periods when large time gaps and/or sharp gradients in the response of O_3 deposition rate to ambient conditions were observed (Yatir summer 2014 and winter 2015).

The fluxes of O_3, CO_2 and water vapor (H_2O), as well as sensible heat (H), latent heat (λE) and momentum were evaluated based on the EC micrometeorological approach (Reynolds, 1894; Stull, 1988). More detailed information on EC theory and application can be found in Aubinet et al. (2012). In addition to the EC measurements, trace gases and complementary meteorological parameters were also measured at all sites. At each site, trace-gas monitors were placed in an air-conditioned mobile laboratory and a tower was used to ensure EC measurements above the roughness sublayer (Szeicz and Long, 1969). In Esh, Bir and Has, a newly designed air-conditioned mobile laboratory was used, designed to overcome limitations in spatial measurement cover using the EC technique, by providing a complete eddy flux system, with adjustable 4–28 m pneumatic tower, power supply and network communication (Asaf et al., 2013; Rohatyn et al., 2018).

Information about the used instrumentation is summarized in Table S1. At all sites except for Shi, we used the following setup for the measurements: a 3D anemometer (R3, Gill Instruments, Hampshire, UK) combined with a closed-path CO_2/H_2O gas analyzer (IRGA; LI-7200, LI-COR, Lincoln, NE, USA), and a fast closed-path dry chemiluminescent O_3 sensor (FOS V2.0.1, Sextant, New Zealand) to quantify H, λE, CO_2 and O_3 flux. Temperature (T), relative humidity (RH), pressure (Campbell Scientific Inc., Logan, UT, USA), solar and long-wave radiation (Kipp & Zonen, Delft, Holland) and photosynthetic radiation sensors (Kipp & Zonen) were also used. In the base of the tower, a mobile laboratory was used to support measurements of several trace gases, including sulfur dioxide (SO_2), nitrogen oxides ($NO_x = [NO] + [NO_2]$) and O_3, using models 43s, 42i and 49i, respectively (Thermo Environmental Instruments Inc., Waltham, MA, USA), with manufacturer-reported limits of detection of 0.1 ppbv, 0.4 ppbv and 1.0 ppbv, respectively. This O_3 measurement (with a manufacturer-reported precision of 1 ppbv) was used to calibrate the 10-Hz measurements by the FOS at a 30-min time resolution. Air was pulled into all closed-path instrumentation using a Teflon tube. The slow-response monitors were periodically calibrated to avoid drift in their accuracy. EC data, except for O_3, were recorded to a CR3000 data logger (Campbell Scientific, Logan, UT, USA), while EC O_3, meteorological data and trace-gas mixing ratios were collected to a computer.

The setup in Shi was similar, except for the following: we used an open-path infrared gas analyzer (Li-7500, LI-COR) to measure CO_2 and H_2O at 10 Hz, and a different 3D sonic anemometer (Gill R3-100). Local T and RH were measured by a Campbell HC2S3 probe, and net radiation was measured by a Kipp & Zonen CNR4 net radiometer, and were recorded by a CR1000 data logger (Campbell Scientific) at 1-min frequency.

2.3. Flux evaluation and partitioning

The methods used for flux evaluation and partitioning are described in this section, with a more detailed description given by Q. Li et al. (2018). The flux evaluation was based on EC methodology, following the equations

$$F = \rho\overline{w'C'} \quad (1)$$

$$H = \rho c_p\overline{w'T'} \quad (2)$$

$$\lambda E = \lambda\rho\overline{w'q'} \quad (3)$$

where F, H and λE are the flux of O_3, and sensible and latent heat, respectively, w is the vertical component of wind speed, ρ is the air density, c_p is the heat capacity of air at constant pressure, T is the air temperature, λ is the vaporization heat of water, and q is the specific humidity. The prime (′) indicates turbulent fluctuation from the mean and the overbar indicates an average over a time period. Mean 30-min fluxes (O_3, CO_2, LE, H) were evaluated using EddyPro 6.2.0 software (LI-COR). Integral turbulence characteristic test was applied based on Foken et al. (1991) to remove data with disturbed or underdeveloped turbulence, resulting in 3.4% of the data with friction velocity (u_*) < 0.1. Stationary quality check was based on Foken and Wichura (1996). We used block average for detrending, double rotation for tilt correction and the despiking method following Vickers and Mahrt (1997). High-frequency-range correction for O_3 flux was applied following Moncrieff et al. (1997). Fratini et al. (2012) was used by default as a high-frequency-range correction for CO_2 and H_2O, except for Shi where the method by Moncrieff et al. (1997) was applied, considering that CO_2 and H_2O fluxes were measured at this site using an open-path sensor. Note that due to insufficiently long measuring periods, at Has, Moncrieff et al. (1997) was also used for the high-frequency-range correction for CO_2 and H_2O, which could result in overestimation of the H_2O flux and therefore F_{tot} partitioning, considering that the H_2O

Table 2
Availability of measured O_3 flux, site and measurement period abbreviations.

Site[a]	Measurement period (yyyy-mm-dd)	Measurement period abbreviation	Total (0.5 h)	Discarded due to incomplete or erroneous data	Available (0.5 h)
Yatir (Yat)	2014-05-12–2014-05-22	Yat-SPR-14	459	201	258
Yatir (Yat)	2014-06-24–2014-08-01	Yat-SUM-14-1	1390	598	792
Yatir (Yat)	2014-08-18–2014-08-28	Yat-SUM-14-2	366	140	226
Yatir (Yat)	2014-09-29–2014-10-10	Yat-AUT-14	482	282	200
Yatir (Yat)	2014-12-04–2014-12-29	Yat-WIN-15-1	928	612	316
Yatir (Yat)	2015-01-25–2015-02-01	Yat-WIN-15-2	380	213	167
Yatir (Yat)	2015-03-24–2015-05-13	Yat-SPR-15	1086	709	377
Birya (Bir)	2013-07-30–2013-08-11	Bir-SUM-13	550	411	139
Birya (Bir)	2014-09-14–2014-09-23	Bir-SUM-14	363	141	222
Eshtaol (Esh)	2014-08-31–2014-09-09	Esh-SUM-14	395	178	217
HaSolelim (Has)	2014-03-12–2014-03-17	Has-WIN-14	241	96	145
HaSolelim (Has)	2014-10-21–2014-10-31	Has-AUT-14	468	298	170
HaSolelim (Has)	2015-03-06–2014-03-15	Has-WIN-15	467	257	210
Shibli (Shi)	2016-10-09–2016-11-07	Shi-AUT-16	1648	1279	369

SPR, spring; SUM, summer; AUT, autumn; WIN, winter.
[a] Site abbreviation appears in parentheses.

flux was used for this partitioning as described below. This potential overestimation is indicated in all figures. Our analyses indicated that this overestimation does not have a significant impact on the diurnal shape of F_{st} or F_{ns}, due to relatively small variation in RH during the day for these measurements. Overall, 41.1% of the measurements were used for O_3 flux evaluation, while the rest of the data were discarded due to measurement incompleteness or failure. Table 2 summarizes the integrated time during each measurement period and information about discarded data.

We used the electrical circuit analogy (Chamberlain and Chadwick, 1953) to partition F_{tot} to F_{st} and F_{ns}:

$$F_{tot} = (C_m - C_0)/(R_a + R_b + R_c) \quad (4)$$

where C_m and C_0 represent the O_3 mixing ratio at the measurement point and near the substomatal cell walls, respectively. C_0 was considered to be 0 based on the assumption that the cell walls act as a perfect O_3 sink (Laisk et al., 1989). R_a is the aerodynamic resistance of turbulent air over the canopy top, R_b is the canopy quasilaminar sublayer resistance to the O_3 flux, and R_c is the canopy resistance to O_3 flux.

The stomatal flux (F_{st}) was calculated as follows

$$F_{st} = \frac{C_c}{R_{st}} = \frac{C_m - F_{tot}(R_a + R_b)}{R_{st}} \quad (5)$$

where R_{st} is the stomatal resistance to O_3. By assuming that gas diffusion is purely molecular inside the stomata, we then calculated R_{st} by multiplying the water vapor stomatal resistance (R_{sw}) by the ratio of the diffusion coefficients for water vapor and O_3 (1.65):

$$R_{st} = 1.65 R_{sw} \quad (6)$$

Using the circuit analogy for water flux (Monteith, 1981), the water stomatal conductance, R_{sw}, was calculated for dry conditions (RH < 65%) as:

$$R_{sw} = \frac{\rho c_p [e_s(T_0) - e(z_m)]}{\gamma \lambda E} - R_a - R_b \quad (7)$$

where $e_s(T_0)$ is the saturation water vapor pressure at the evaporation surface temperature T_0, $e(z_m)$ is the water vapor pressure at the measurement height z_m, γ is the psychrometric constant (67 Pa K^{-1}), and λE is the measured latent heat.

To extend this application to wet conditions, we assumed that there is a strong correlation between gross primary productivity (GPP) and stomatal conductance to water (g_{sw}), considering that they are both predominantly controlled by stomatal opening (Farquhar and Sharkey, 1982). First, we evaluated the regression between the two under dry conditions, assuming that under those conditions, when surface evaporation is limited, g_{sw} can be evaluated from the daytime-evaluated GPP (Lamaud et al., 2009; Stella et al., 2011). Then we used the coefficients for the regression between g_{sw} and GPP under dry conditions to evaluate g_{sw} from GPP under non-dry conditions.

Since the vegetation at all sites was dominated by C3 plants, the evaluation of g_{sw} was based on an exponential regression between g_{sw} and GPP under dry conditions (Lamaud et al., 2009; Stella et al., 2011). The evaluation of GPP during the day was based on subtracting the evaluated respiration flux from the measured CO_2 flux, individually for each diurnal cycle (see Q. Li et al., 2018). Under the studied conditions, regression was always performed for RH < 65%, whereas in winter, regression was performed only for measurements at least 24 h after any rain event.

It should be noted that decoupling of GPP and g_{sw} can occur due to limited carboxylation, which is not directly related to stomatal conductance, such as in the case of incomplete nighttime stomatal closure in C3 plants or during intense light or exposure to O_3 (Caird et al., 2007; Lombardozzi et al., 2012; Maier-Maercker and Koch, 1991; Paoletti, 2005; Paoletti and Grulke, 2005; Pearson and Mansfield, 1993; Tjoelker et al., 1995; Wilkinson and Davies, 2009). Considering that the level of decoupling is expected to vary with leaf age and season (e.g., Panek, 2004; Stella et al., 2011), it is important that both the regression and its application to non-dry conditions be for a short enough period of time.

It is also noted that for Has in winter, a linear regression between g_{sw} and GPP was used, to avoid an unrealistic bias in calculated F_{st} due to outliers. Hence, in this respect, some of the highest evaluated F_{st} may be underestimated, as indicated in all figures.

2.4. Large-scale atmospheric data

Atmospheric data were analyzed to diagnose the large-scale atmospheric environment, and the association of dry intrusions (DIs) with the extreme surface dry events, as follows. Data are taken from the European Centre for Medium-range Weather Forecasts (ECMWF) ERA-Interim reanalysis (Dee et al., 2011). Wind, temperature and humidity data are available 6-hourly at 1° horizontal resolution and 60 hybrid vertical levels. O_3 mixing ratio data are available from the assimilation of satellite retrievals in the reanalysis (Dee and Uppala, 2009; Dragani, 2011). Planetary boundary layer (PBL) height is estimated using the mass flux/eddy diffusivity concept, using different K closures for different PBL regimes (ECMWF, 2007). Large-scale dry air intrusions (DIs) are diagnosed in a Lagrangian framework, by calculating air mass trajectories according to the ERA-Interim wind field using the Lagrangian Analysis Tool LAGRANTO 2.0 (Sprenger and Wernli, 2015). The identification of dry intrusion trajectories requires a vertical descent of at least 400 hPa during 48 h, resulting in deeply slantwise-descending airstreams. A global DI dataset has been compiled recently (Raveh-Rubin, 2017), while here, DI trajectories present within a 1°-distance from 31°N, 35°E, are identified.

3. Results and discussion

3.1. O_3 flux and partitioning

F_{tot} averaged −5.6 to −13.2 nmol m^{-2} s^{-1} during the winter and − 6.0 to −10.4 nmol m^{-2} s^{-1} during the spring, summer and autumn. While these values agree well with values reported in the Western Mediterranean (see Table 2 in Q. Li et al., 2018), F_{st}/F_{tot} was lower than 50% and reached extremely low values during the autumn (9–30%), and even more so in Yat during the summer (8–11%). F_{tot} in Yat increased gradually from winter to summer and decreased gradually from summer to autumn. Summer, when F_{tot} in Yat reached its maximum, was the only time that it was comparable in magnitude to summertime F_{tot} at other sites. The fact that F_{st}/F_{tot} in Yat reached very low values in summer may be considered a positive property for a forest, in that it reflects a high rate of O_3 removal, with minimal fraction of F_{st} which is associated with minimal negative effects on vegetation and a reduction in carbon assimilation (see Section 1). The F_{ns}/F_{tot} fraction in Yat increased relatively sharply from 8% to 38% between winter and summer, and then decreased to ~21% at autumn. Overall for all measurements, vapor-pressure deficit (VPD) tended to anticorrelate ($r^2 = 0.72$) with F_{st} during winter to early summer, but less so during late summer and autumn, reflecting a strong limitation on vegetation activity, even during winter and spring, and decoupling between VPD and F_{st} during summer and autumn ($r^2 = 0.06$), when soil water availability probably dominates the vegetation activity (see Section 3.3).

While no clear trend along the ICG was observed for F_{tot} (see Fig. 2) or F_{ns} (not shown here), Fig. 2 clearly indicates that during the summer, F_{st} decreased with aridity following the order Bir > Esh > Yat. The strong limitation on F_{st} in Yat was evidenced by the fact that in the spring, it was lower than in the summer at the other sites.

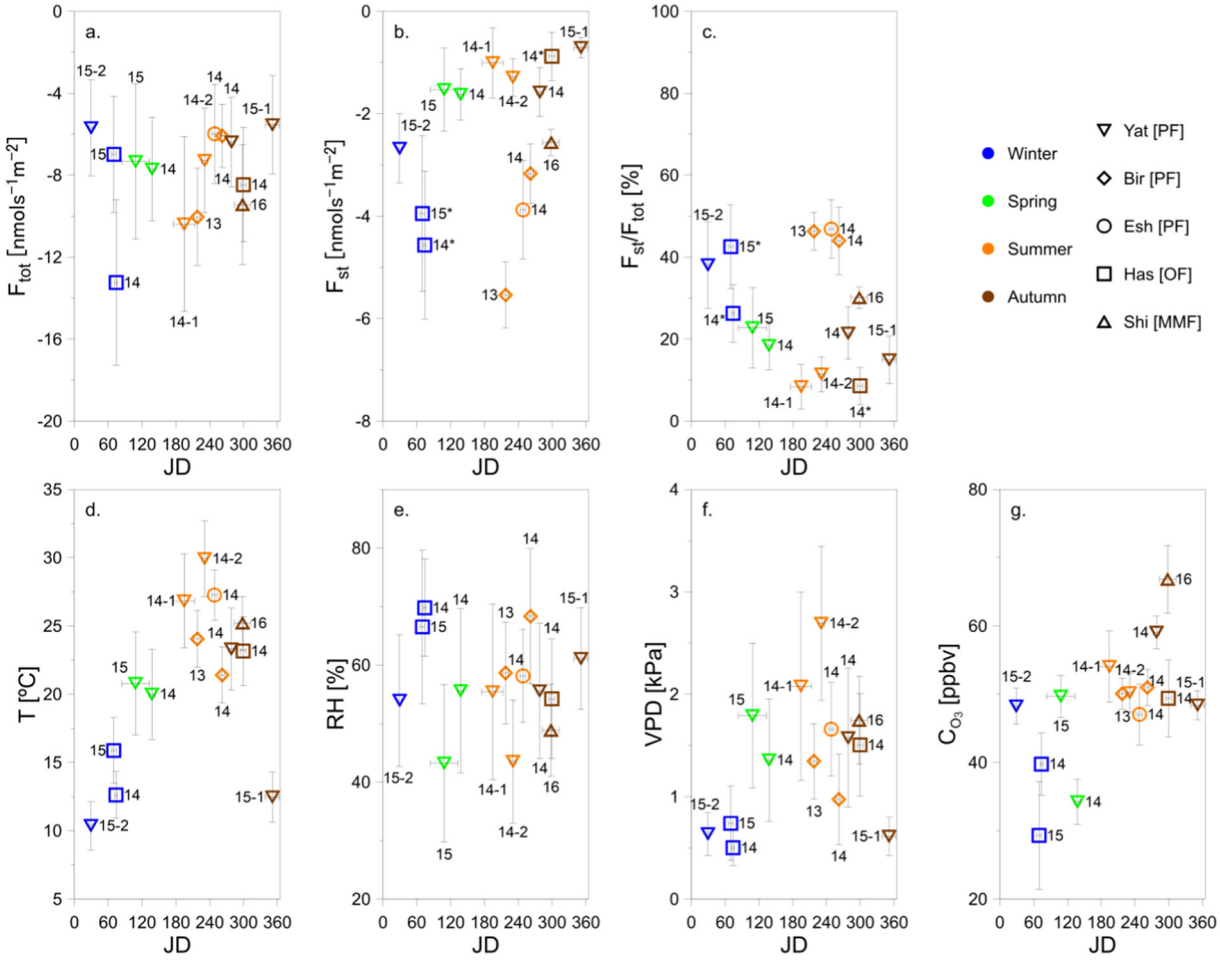

Fig. 2. Ambient conditions, O_3 flux and its partitioning. Presented are (a) total O_3 flux (F_{tot}), (b) stomatal flux (F_{st}), (c) F_{st}/F_{tot}, (d) temperature (T), (e) relative humidity (RH), (f) vapor-pressure deficit (VPD) and (g) O_3 mixing ratios (C_{O_3}). Different sites, vegetation and seasons are represented by different symbols and colors (see Tables 1 and 2 for abbreviations), respectively. Vertical error bars represent standard deviation, and horizontal bars represent measurement duration. JD, median Julian day during the measurement period. *See Section 2.3 for potential inaccuracies in F_{tot} partitioning.

3.2. Diurnal profiles of F_{tot}, deposition velocity (V_d) and F_{st}/F_{tot}

Fig. 3 presents the average diurnal profiles of F_{tot}, V_d and F_{st}/F_{tot}, individually for the different measurement periods. The figure indicates positive F_{tot} during several measurement periods, including Yat-SPR-15, Yat-WIN-15-1, Shi-AUT-16 and Esh-SUM-14, which we attribute to DI from the upper atmosphere and anthropogenic NO from elevated sources, as will be discussed in Sections 3.4.1 and 3.4.3. Fig. 3 also indicates that the ratio between daytime and nighttime deposition rate tends to be minimal from autumn to early spring, and higher during late spring and summer. While on average, daytime V_d (V_d-d) in late spring and summer was higher than nighttime V_d (V_d-n) by ~74%, the corresponding value during late autumn and early winter was ~8%. Note that during Yat-WIN-15-1, V_d-n was higher than V_d-d. To some extent, this can be attributed to positive F_{tot}, but additional factors played a role in this trend, inducing the relatively high nighttime vs. daytime O_3 deposition during this measurement period and others, as will be discussed in Sections 3.4.2 and 3.4.4.

The seasonal and diurnal distributions of F_{st}/F_{tot} are important properties, considering the significant diurnal and seasonal O_3 mixing ratio (C_{O_3}) cycles. Ideally, lower F_{st}/F_{tot} during higher C_{O_3} will result in efficient O_3 removal from the troposphere, with minimal accompanying negative impact on the plants and climate (Section 1). Fig. 3 indicates that in Yat, F_{st}/F_{tot} tended to reach maximal values around noon only during Yat-WIN-15-2, whereas from spring until early winter (Yat-Win-15-1), maximum F_{st}/F_{tot} tended to occur in the morning and evening, with minimal values around noon. This F_{st}/F_{tot} distribution suggests a large benefit in terms of O_3 removal with minimal associated negative effects on climate and vegetation, considering that C_{O_3} tends to be minimal during the winter (Fig. 2) and its diurnal maximum typically occurs at around noon or in the afternoon (e.g., see Fig. 4). Note that one exception is Yat-SPR-14 (Fig. 2), for which lower than usual C_{O_3} levels were recorded due to higher than usual titration of O_3 by NO. In contrast to Yat, at the other pine sites, Bir and Esh, the fraction tended to be maximal or relatively high at around noon, with F_{st}/F_{tot} ~ 40–60% (Fig. 3h–j).

3.3. Impact of environmental conditions on stomatal conductance

To further investigate the impact of environmental conditions on F_{st}, we investigated its response to changes in C_{O_3} and O_3 stomatal conductance (G_{st}), as well as the latter's response to changes in VPD and photosynthetically active radiation (PAR). Fig. 4 presents, for each measurement period, the average diurnal profile of F_{st} vs. the corresponding C_{O_3} and G_{st}, and of G_{st} vs. the corresponding VPD and PAR. The corresponding Pearson correlation coefficient (PCC) and average values of all variables are also presented. Fig. 4 demonstrates a general decrease in G_{st} at Yat when shifting from winter to summer, with even lower values during the autumn and early winter, prior to winter precipitation (Yat-WIN-15-1). At the other sites, measurements were limited to a single season, except for Has, where significantly lower G_{st}

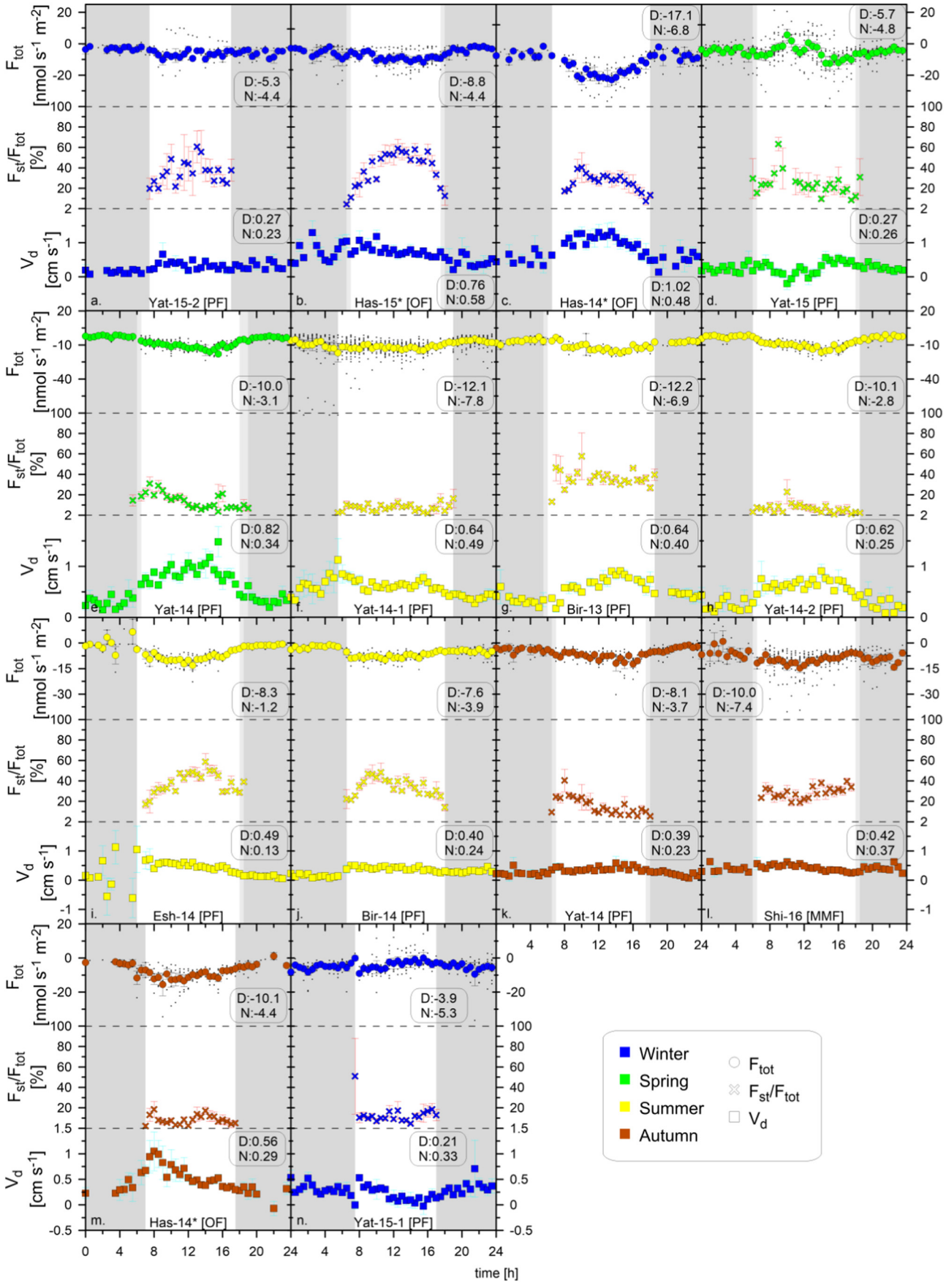
a. Yat-15-2 [PF]
b. Has-15* [OF]
c. Has-14* [OF]
d. Yat-15 [PF]
e. Yat-14 [PF]
f. Yat-14-1 [PF]
g. Bir-13 [PF]
h. Yat-14-2 [PF]
i. Esh-14 [PF]
j. Bir-14 [PF]
k. Yat-14 [PF]
l. Shi-16 [MMF]
m. Has-14* [OF]
n. Yat-15-1 [PF]
F_tot [nmol s-1 m-2]
F_st/F_tot [%]
V_d [cm s-1]
time [h]
Winter
Spring
Summer
Autumn
F_tot
F_st/F_tot
V_d

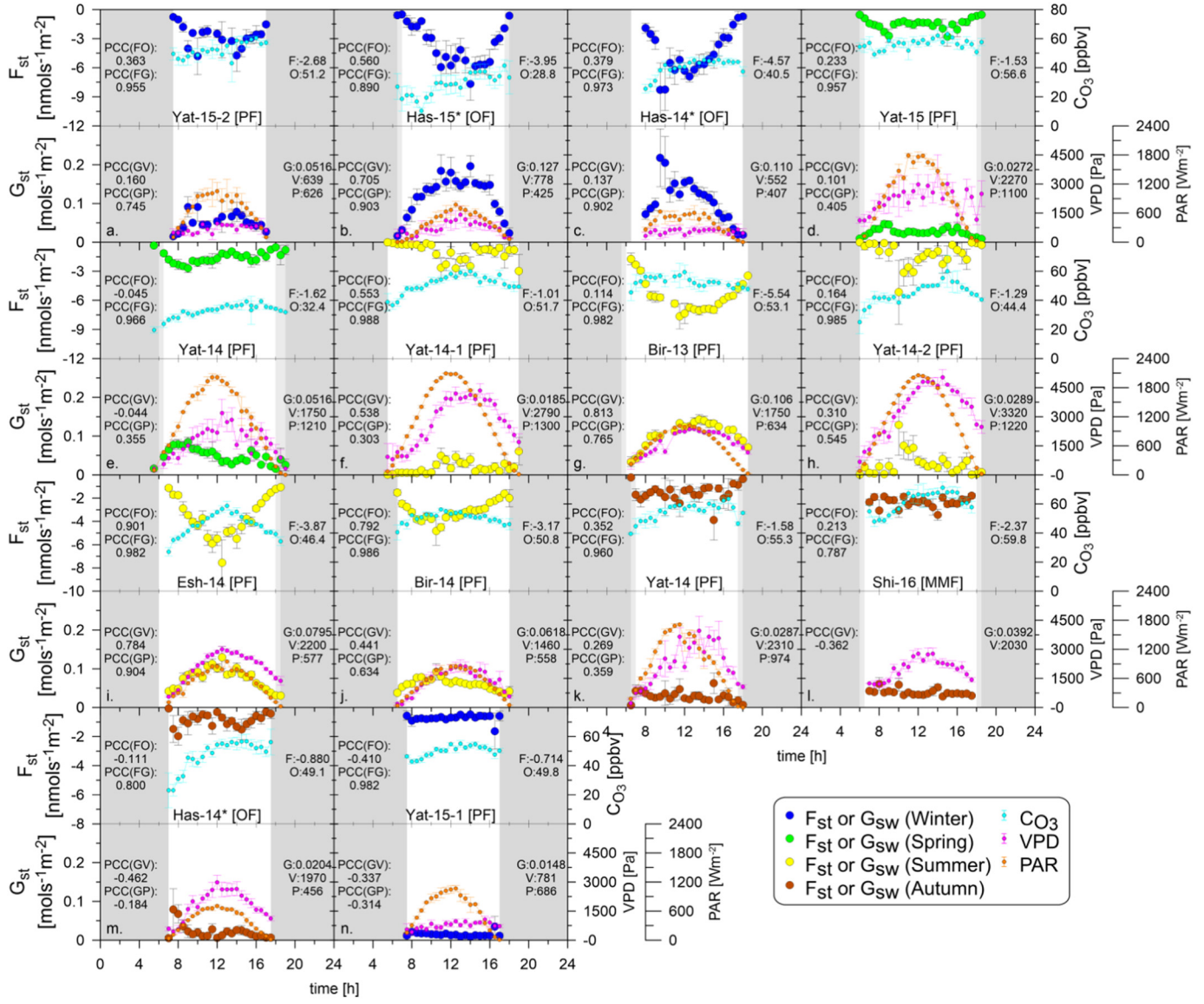

Fig. 4. Potential impact of O_3 mixing ratio (C_{O_3}), stomatal O_3 conductance (G_{st}), vapor-pressure deficit (VPD) and photosynthetically active radiation (PAR) on the diurnal profile of stomatal O_3 flux (F_{st}). For each measurement period, the figure presents the average F_{st} and C_{O_3} vs. time (upper panel) and average G_{st}, VPD and PAR vs. time (lower panel); see Tables 1 and 2 for site and measurement period abbreviations. The darker and lighter shaded areas represent, respectively, nighttime for the entire measurement period, and nighttime for part of the measurement period, due to changes in daylight hours during the year. The Pearson correlation coefficients (PCCs) between F_{st} and C_{O_3} [PCC(FO)], Fst and G_{st} [PCC(FG)], Gst and VPD [PCC(GV)], and G_{st} and PAR [PCC(GP)], as well as the integrated values of F_{st} (F), C_{O_3} (O), G_{st} (G) and VPD (V) are also presented individually for each measurement period. *See Section 2.3 for potential inaccuracies in F_{tot} partitioning.

was also obtained during the autumn vs. winter. While the decrease in G_{st} from winter to spring in Yat may be explained by a corresponding increase in VPD, the decrease in G_{st} from summer to early winter seems to be caused by limited soil water availability, considering that VPD during the autumn and early winter was comparable or lower than that in summer in Yat. This is in agreement with the discussed relationship between VPD and F_{st} based on Fig. 2, as well as with previous studies (Anav et al., 2016; Anav et al., 2018b; de Marco et al., 2016).

Fig. 4 also enables exploring the response of the average diurnal profile of G_{st} to PAR and VPD. In general, the diurnal profile of G_{st} is expected to be controlled by both factors. Because both negative and positive correlations between G_{st} and VPD can occur during a specific measurement period, and even on a specific day, canceling each other out, PCC between VPD and G_{st} may not be sufficiently representative of the correlation between the two. Hence, the effect of VPD on G_{st} may be better identified, indirectly, by the PCC between PAR and G_{st}, which is expected to decrease under higher impact of VPD. Fig. 4 clearly indicates a general decrease in PCC for G_{st} vs. PAR from winter to summer, and negative values during the autumn and early winter (Yat-WIN-15-1), indicating a corresponding influence of VPD on G_{st}.

To further investigate the response of G_{st} to VPD, Fig. 5 presents scatter plots of G_{st} vs. VPD, individually marking morning (yellow), noon (pink) and evening (cyan). During the winter, G_{st} did not show any significant dependence on VPD, as indicated by the high PCC for G_{st} vs. PAR (Fig. 4) and by comparing Fig. 5 with Fig. S1. During the spring, midday dispersion in G_{st} was observed in Yat (Fig. 4d,e), suggesting significant

Fig. 3. Diurnal profiles of total O_3 flux (F_{tot}), its stomatal fraction (F_{st}/F_{tot}) and deposition velocity (V_d). Presented are the average diurnal profiles of F_{tot}, F_{st}/F_{tot} and V_d, separately for each measurement period (a–n; see Tables 1 and 2 for site and measurement period abbreviations). Colored points represent the half-hourly average values. Different colors represent different seasons (see key on figure). The darker and lighter shaded areas represent, respectively, nighttime for the entire measurement period, and nighttime for part of the measurement period, due to changes in daylight hours during the year. *See Section 2.3 for potential inaccuracies in F_{tot} partitioning.

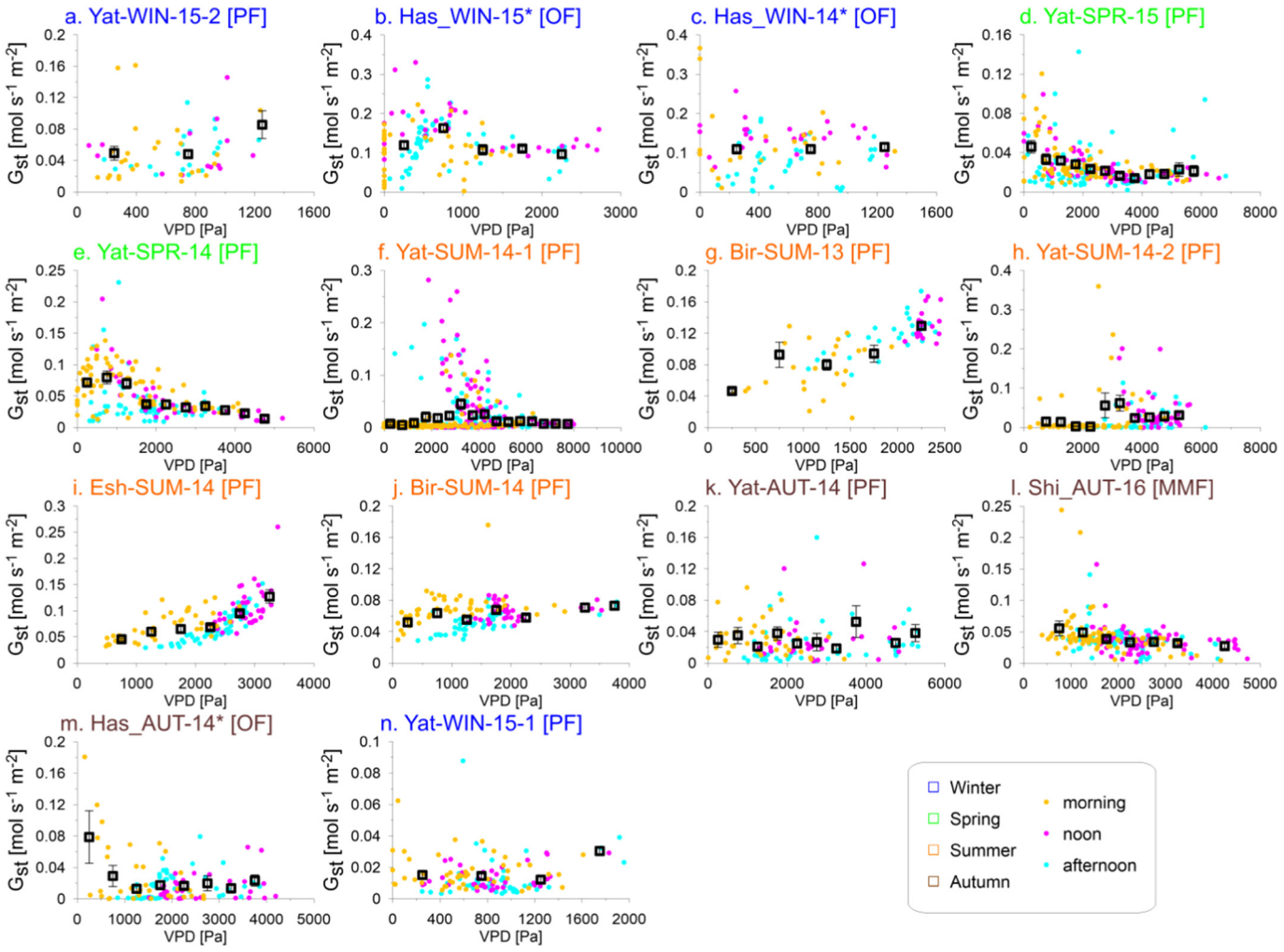

Fig. 5. Response of O_3 stomatal conductance (G_{st}) to vapor-pressure deficit (VPD) during the day. Points present G_{st} vs. VPD, individually for each measurement period (a–n; see Tables 1 and 2 for site and measurement period abbreviations), while points in the morning, noon and evening are indicated by orange, pink and cyan color, respectively. Squares represent bin-based averaging (see Section S7) of G_{st} vs. VPD. Vertical bars represent standard error of the mean, associated with each bin. *See Section 2.3 for potential inaccuracies in F_{tot} partitioning.

anticorrelation between G_{st} and VPD, at least around noontime (Fig. 5d, e). During Yat-SUM-14-1, midday depression occurred on some days as high VPD around noon (Fig. 5f), whereas during Yat-SUM-14-2, depression in G_{st} occurred throughout most of the day, except for the morning (Fig. 5h). In autumn and early winter, G_{st} in Yat was low throughout the day (Fig. 4).

Whereas in Yat, a positive correlation between G_{st} and VPD was observed only in winter, for VPD > ~1000–1200 Pa (Fig. 5) in Bir and Esh, a positive correlation between G_{st} and VPD was also observed in summer, with comparable PCC for G_{st} vs. VPD and PAR (Fig. 4) and highest G_{st} corresponding to highest VPD around noon (Fig. 5). However, in late summer, the positive correlation between G_{st} and VPD in Bir (Bir-SUM-14) was significantly smaller (Figs. 4j, 5j).

Similar to G_{st}, F_{st} decreased sharply in Yat from winter to autumn and early winter, prior to precipitation (Yat-WIN-15-1). F_{st} is directly controlled by both C_{O_3} and stomatal conductance (see Eq. (5)). Using G_{st} as a measure for stomatal conductance it appears, by comparing PCC for F_{st} vs. G_{st} with PCC for F_{st} vs. C_{O_3} (Fig. 4), that F_{st} during all measurement periods was dominantly controlled by stomatal conductance rather than by C_{O_3}. Comparable PCCs for F_{st} vs. C_{O_3} and F_{st} vs. G_{st} were obtained only in the late summer for Esh-SUM-14 and Bir-SUM-14, which may also result from the high correlation between G_{st} and C_{O_3} during these measurements (Fig. 4). In the winter, a relatively strong impact of C_{O_3} on F_{st} was also observed in Yat and Has (see Fig. S5). The generally weak impact of C_{O_3} under warm and dry conditions is consistent with findings based on modeling and observation studies, which suggested a strong drought-induced limitation of stomatal O_3 uptake in the Mediterranean region (Emberson et al., 2007; Fares et al., 2010b; Matyssek et al., 2007).

The fact that stomatal conductance was not limited by drought in Yat in the winter, together with the fact that C_{O_3} does not play a significant role in F_{st} magnitude under drought conditions, resulted in a clear decreasing integrated F_{st} in Yat following the order winter > spring > summer > autumn/early winter (see Fig. 2). C_{O_3} was comparable at all investigated sites (see also Fig. 4) and tended to be highest during the warm seasons. Therefore, the yearly integrated F_{st} in Yat is expected to be low compared with Bir and Esh, as is also implied by Fig. 2. The relatively high stomatal conductance in Bir and Esh during the summer, corresponding with the relatively high C_{O_3}, resulted in a high F_{st}, even in summer, and most likely during the spring when C_{O_3} in this region is also very high (Dayan and Levy, 2002).

3.4. Impact of environmental conditions on non-stomatal conductance (G_{ns})

3.4.1. Reaction with NO

In vegetated areas, NO can be emitted from the soil and vegetation, and its subsequent reaction with O_3 can stimulate the latter's deposition. The emission of NO from soil is enhanced by T (Q_{10} of about 2, indicating double the emission rate for a 10 °C increase in temperature;

Williams et al., 1992). Hence, soil emission of NO contributes significantly to O_3 deposition under Mediterranean conditions (Fares et al., 2012; Farmer and Cohen, 2008; Kurpius and Goldstein, 2003) and under semiarid conditions, subject to soil water availability (Meixner and Yang, 2006). NO can also be emitted from vegetation at a rate comparable to its emission from the soil (Wildt et al., 1997). A recent study in the Eastern Mediterranean revealed that NO emission above vegetation from elevated anthropogenic sources can result in reduced O_3 deposition rate to vegetation and even an upward F_{tot} (Q. Li et al., 2018). The analysis used for the present study indicates that emission of NO from elevated anthropogenic emission sources probably reduced O_3 deposition rate for Has-WIN-14 and Bir-SUM-13 and led to positive F_{tot} events for Bir-SUM-13 (see Fig. 3), Shi-AUT-16 and Esh-SUM-14 (-Section S9). Overall, our analyses revealed that NO does not play a significant role in affecting O_3 deposition (see Section S9), and the analyses presented in the following sections confirm the notion that other factors play more significant roles.

3.4.2. Temperature and RH

In this section, we study the impact of T and RH together on non-stomatal O_3 deposition because these parameters tend to anticorrelate. Under the high temperatures in Mediterranean areas, gas-phase reaction of O_3 with biogenic volatile organic compounds (BVOCs) has been found to play a major factor in non-stomatal O_3 deposition, due to the generally exponential growth of BVOC emission rate with T (Bouvier-Brown et al., 2009; Fares et al., 2009, 2010b, 2012; Goldstein et al., 2004; Guenther et al., 1993; Kurpius and Goldstein, 2003; Owen et al., 1997; Richards et al., 2013). Note that BVOC emission rate in Mediterranean regions can also be enhanced by solar radiation, and either enhanced or affected differently by other abiotic stress factors, such as drought and oxidative stress conditions (e.g., by O_3 uptake) (Loreto and Schnitzler, 2010; Staudt and Seufert, 1995). It should also be noted that the BVOC-induced O_3 deposition to vegetation may not be confined only to gas-phase reactions, but may also be facilitated by chemical reaction at the leaf surface or by stimulated formation of a waxy layer on the leaf, which can take up and chemically react with O_3 (Altimir et al., 2006; Gerosa et al., 2009; Massman, 2004). In addition to BVOC emission, other processes that are stimulated by T can enhance the deposition rate of O_3 to vegetated areas, such as soil emission of NO as discussed in Section 3.4.1, and the thermal decomposition of O_3 on surfaces (Fowler et al., 2001), which will be discussed further on in this section.

RH can enhance non-stomatal deposition of O_3 by stimulating the formation of leaf surface wetness. While the uptake of O_3 by pure water is too slow to significantly affect its gas-phase concentration (Jacob, 2000), efficient deposition of O_3 to wetted vegetation surfaces has been reported, where water films can be formed, and potentially induced by a waxy layer and other dissolved salts which can further react with O_3 (Altimir et al., 2006; Cape et al., 2009). The occurrence and/or efficiency of O_3 uptake by the wetted surface is further dependent on the latter's chemical reactivity, the presence and characteristics of wax, and leaf properties (Massman, 2004). The enhancement of O_3 uptake by increasing surface wetness has been found to increase hyperbolically with increasing RH for RH > 70% (Altimir et al., 2004; Altimir et al., 2006; Gerosa et al., 2009; Lamaud et al., 2002). This implies generally low efficiency of the mechanism during the day, under the relatively low RH in Mediterranean areas. However, Q. Li et al. (2018) recently observed a significant increase in O_3 deposition rate to vegetation for RH well below 70% near the Eastern Mediterranean shore, most probably resulting from deposition of marine aerosols on leaves, combined with BVOC emission.

Fig. 6 presents G_{ns} vs. both T and RH during the night. The figure indicates a general increase in G_{ns} with RH for all measurements. In contrast to most previous studies, in some cases, an increase in G_{ns} occurred in Yat for RH < 70% as well (e.g., Yat-SPR-15, Yat-SPR-14, Yat-SUM-14-2 and Yat-WIN-15-1; Fig. 6d, e, h and n, respectively), although the increase was not always monotonic. The significant increase in G_{ns} for RH < 70% suggests the involvement of marine aerosols in stimulating surface wetness formation, following their deposition on the leaves (see Q. Li et al. (2018) and Burkhardt and Eiden, 1994). A recent study has indicated that sea breeze transports, on a daily basis, marine aerosols to a desert site, 80 km away from the Eastern Mediterranean seashore, during the day in the summer (Derimian et al., 2017). The sea breeze also leads to an increase in water vapor content and RH which, in turn, lead to a shift in aerosol size distribution toward larger aerosols. Hence, we expect that marine aerosols can potentially induce surface wetness in Yat, ~59 km from the seashore. The transport of marine aerosols under low RH becomes feasible due to the lowering of the Aerosols' deliquescence RH to even <40% by uptake of certain minerals such as $MgCl_2$ or $CaCl_2$ (Gupta et al., 2015; Metzger and Lelieveld, 2007; Tang et al., 1997; Zieger et al., 2017).

During Yat-SPR-14 and Yat-SUM-14-2, air masses were transported from the sea during the night, at least part of the time. During Yat-WIN-15-1 and Yat-SPR-15, air masses were transported to the site from the east (see Fig. S3) and for these cases, it is possible that marine aerosols which were previously transported from the sea eastward during the afternoon were transported to the site by the prevailing nighttime easterly winds. Such recirculation events for air masses are frequent in this region (Alper-Siman et al., 1997; Dayan et al., 2017; Dayan and Rodnizki, 1999; Feliks, 1991). It may also be that aerosols other than sea salt are involved in stimulating a wetted surface on the vegetation's leaves, such as mineral dust, organic aerosols and sulfate aerosols, which can also retain water at relatively low RH (Abdelkader et al., 2017; Hersey et al., 2009; Metzger and Lelieveld, 2007).

At sites other than Yat, there was no indication of an increase in G_{ns} with RH for RH < 70%. In part, this could be explained by insufficient measurements at RH < 70% at these sites during the night. In the case of Bir-SUM-13, westerly winds predominated during the night along with RH well below 70%, and in this case the apparent absence of an aerosol impact on O_3 deposition may be due to different aerosol composition. For instance, exposure of aerosols to primary air pollution, such as sulfur and nitrogen oxides, tends to increase the aerosols' acidity, which in turn can significantly reduce O_3 uptake to the aqueous phase prior to and following the aerosols' deposition on the leaves (Chameides and Stelson, 1992; Keene, 2002; Keene and Savoie, 1998; Pszenny et al., 2004). Another reason might be the higher emission rate of BVOCs at low RH, corresponding with high T, during the night (Holzinger et al., 2005). The latter is supported by the much higher (by a factor of 5–8) emission rate of terpene in Bir compared to Yat during the summer (Llusia et al., 2016; Seco et al., 2017). Fig. 6 indicates a general decreasing trend of G_{ns} with T during the winter and spring, and an opposite trend during Bir-SUM-13, Esh-SUM-14 and Yat-AUT-14. This seasonal effect of a higher tendency toward increasing G_{ns} with T during the summer and early autumn points to a contribution of BVOC emission during these warmer seasons, indicating that BVOC emission plays a more important role in O_3 deposition than the other aforementioned T-induced mechanisms.

Fig. 7 provides the same information presented in Fig. 6, but for daytime. A clear increase in G_{ns} with T only occurred during Bir-SUM-13, reinforcing the relatively strong BVOC emission at this site. During several other measurement periods in spring and summer, however, an increase in G_{ns} with T was observed for the higher T range, most clearly during Yat-SPR-15 and Yat-SPR-14. On the other hand, in the lower T range, associated with RH > 70%, an increase in G_{ns} with RH was observed in most cases, indicated by the trend lines in Fig. 7. The tendency toward increasing G_{ns} with RH, for RH > 70%, indicates a dominant effect of RH-induced surface wetness formation for RH > 70%, whereas for the lower RH and higher T range, the effect of T, particularly during the spring and summer, tends to dominate. It should also be noted that the fact that an increase in G_{ns} with T is observed for the higher T range in Yat only during the spring, and not during the summer or autumn, agrees with the strong limitation on monoterpene emission at

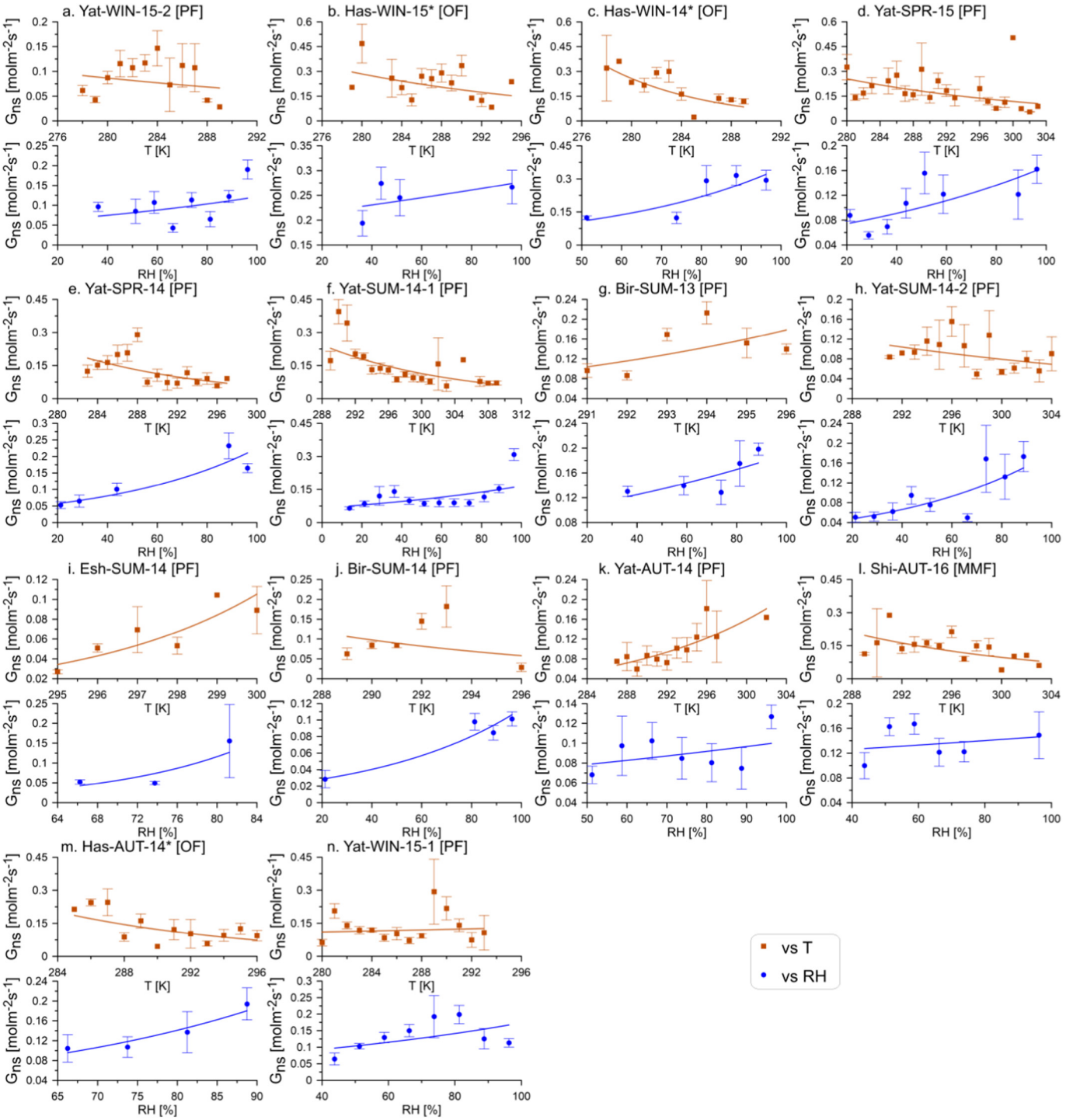

Fig. 6. Response of non-stomatal O_3 conductance (G_{ns}) to temperature (T) and relative humidity (RH) during the night. Upper and lower panels in each section present bin-based averaging of G_{ns} vs. T and G_{ns} vs. RH (Section S7), respectively, and the corresponding exponential non-linear fitting curve for each measurement period (see Tables 1 and 2 for site and measurement period abbreviations). Note that only bins with at least 5 data points per bin were included in the graphs and analysis. Vertical bars represent standard error of the mean, associated with each bin. *See Section 2.3 for potential inaccuracies in F_{tot} partitioning.

this site under strong drought conditions, whereas in Bir, BVOC emission is enhanced during the summer (Seco et al., 2017).

Fig. 8 presents the integrated impact of T and RH on G_{ns} during the different measurement periods, by showing the bin-based exponential regression slope coefficient (ERSC) and the corresponding coefficient of determination (r^2) for the regression of G_{ns} vs. RH and G_{ns} vs. T, for each measurement period and individually for nighttime and daytime. Overall, the figure clearly demonstrates high sensitivity of G_{ns} to RH during both day and night, which tended, in general, to be significantly higher than the sensitivity of G_{ns} to T.

The high drought limitation and relatively high impact of RH on F_{tot} under the present study conditions resulted in F_{tot} and F_{st}/F_{tot} diurnal profiles that differed from those typically observed in other Mediterranean areas. The relatively strong impact of RH near the Mediterranean

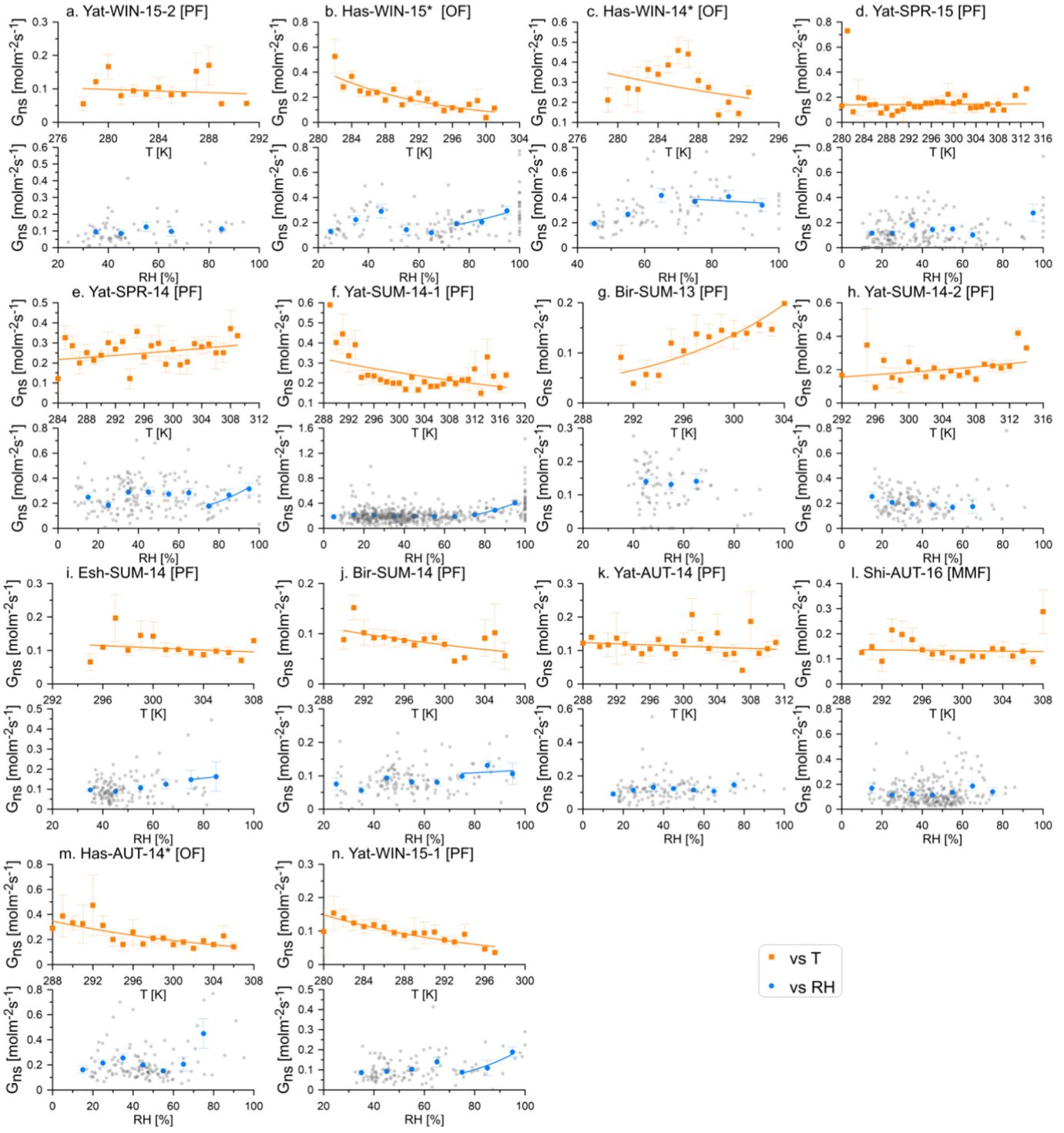

Fig. 7. Response of non-stomatal O_3 conductance (G_{ns}) to temperature (T) and relative humidity (RH) during the day. Upper and lower panels in each section present bin-based averaging of G_{ns} vs. T and G_{ns} vs. RH (Section S7), respectively, and the corresponding bin-based (see Section S7) exponential non-linear fitting curve for each measurement period (see Tables 1 and 2 for site and measurement period abbreviations). Note that only bins with at least 5 data points per bin were included in the graphs and analysis. In the case of G_{ns} vs. RH, fitting curves are only presented for RH ≥ 70%. Vertical bars represent standard error of the mean, associated with each bin. *See Section 2.3 for potential inaccuracies in F_{tot} partitioning.

coast, compared to other environmental factors, together with the generally high nighttime air mixing (see Section 3.4.4), is a major reason for the relatively small V_d-d/V_d-n (Section 3.2). Previous studies in Mediterranean areas have indicated peak F_{tot} around noon and in the early afternoon, predominantly due to maximum F_{st} and a large contribution of F_{ns} during this time (Fares et al., 2010a; Fares et al., 2010b; Fares et al., 2012; Kurpius and Goldstein, 2003). Under the conditions of the present study, a peak in F_{tot} was also observed around noon and in the early afternoon (Fig. 3), but in most cases this peak was much less intense compared to other studies under Mediterranean conditions, and in some cases, there was no clear difference between the magnitude of F_{tot} at this time and during the rest of the day (e.g., Yat-SUM-14-1; Fig. 3).

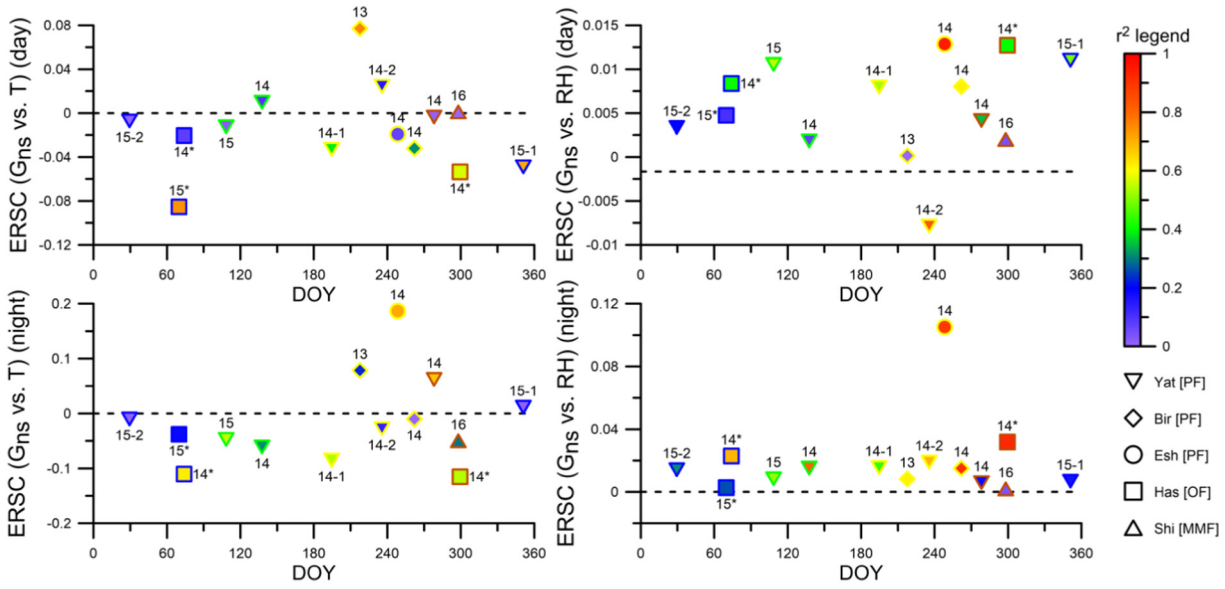

Fig. 8. Response of non-stomatal O_3 conductance (G_{ns}) to changes in temperature (T) and relative humidity (RH). Presented are the exponential regression slope coefficient for the bin-based regression (see Section S7) between G_{ns} vs. T (left panels) and RH (right panels) during the day (upper panels) and at night (lower panels), respectively. Different sites and seasons are represented by different symbols and line colors, respectively. Labels represent the measurement period (see Tables 1 and 2 for site and measurement period abbreviations). The filling color represents the regression's corresponding r^2 value (see color key on figure). Dashed line represents the zero line of the slope. *See Section 2.3 for potential inaccuracies in F_{tot} partitioning.

We attribute this to low stomatal conductance and high limitation of F_{st}, together with the high impact of RH on F_{ns}, which tends to be lowest around noontime.

3.4.3. Extreme dry surface events

During three measurement periods in Yat—Yat-WIN-15-2, Yat-SPR-15 and Yat-WIN-15-1—positive F_{tot} events were observed (see Fig. 3). These events cannot be explained by NO from elevated emission sources, in those cases for which NO_X measurements were available. In all cases, the positive F_{tot} events were accompanied by extremely low daytime RH near the surface, which typically lasted several days. Fig. 9 presents the positive F_{tot} events together with the measured RH and RH gradient for two different periods during Yat-SPR-15. To understand the evolution of surface RH during the 4 weeks of Yat-SPR-15, we examined the large-scale variation of specific and relative humidity in the tropospheric column, from the surface up to the lower stratosphere (100 hPa), at 31°N 35°E using the ERA Interim reanalysis (Fig. 9a).

The extremely low surface RH event between 26 and 30 April is characterized by low RH throughout the troposphere, and is in fact preceded by yet drier air masses above the PBL on 23–24 April, which subsequently penetrated the PBL on 25 April. These dry air masses followed a trajectory that fulfills the Lagrangian definition of the so-called DI (see Fig. S7), indicated by the black dots in Fig. 9a. The DI air masses typically descend substantially slantwise from the upper troposphere to the middle and low troposphere, while propagating toward the equator, often in association with the passage of a cyclone's cold sector (Browning, 1997; Raveh-Rubin and Wernli, 2016; Wernli, 1997). The DIs here started their descent from ~400 hPa near Western Russia on 00 UTC 23 April, and descended to the lower troposphere while moving southward until they reached the Middle East on 00 UTC 25 April (Fig. S7a). The shorter dry surface event during 19–21 April was also preceded by a DI, although it was less pronounced.

The DI events presented here were all followed by extremely low surface RH events, during which positive F_{tot} events occurred on a daily basis for RH < 25% (indicated by dark blue in Fig. 9b). Note that on 19–20 April, no measurements were available to explore whether the RH < 25% at the surface was accompanied by positive F_{tot}. We suggest that the positive F_{tot} events occurred due to a decrease in the canopy's effectiveness to act as a sink for O_3 under the extremely dry conditions, and the existence of more humid air higher in the PBL. The relatively small vertical RH gradient near the surface during the positive F_{tot} events implies that the extreme dryness extended at least a few dozen meters above ground (Fig. 9c), likely also limiting the water-retention ability of aerosols and salts near and on the surface to retain water, thereby significantly reducing the uptake of O_3 by the canopy. Fig. 9a indicates higher RH further up in the PBL, between 26 and 28 April, where aerosols may be able to retain water and act as a more efficient sink for O_3 than the canopy, resulting in lower C_{O_3} further up in the PBL than near the surface, and leading, in turn, to a positive O_3 flux.

Note that we could not identify the occurrence of DI events for all other positive O_3 events during Yat-WIN-15-1 and Yat-WIN-15-2, although in this region, DI occurrence peaks in the winter and spring (Raveh-Rubin, 2017). This may be due to the strict criteria used by ERA Interim for the definition of a DI event, i.e., a 400 hPa descent within 48 h. The fact that RH was shown to play a major role in the studied area together with the strong limitation on BVOC emission from the vegetation under severe drought conditions (Llusia et al., 2016) can certainly play a key role in the positive F_{tot} events.

3.4.4. C_{O_3} and friction velocity (u_*)

Atmospheric stability and C_{O_3} are basic factors controlling O_3 dry deposition, also when surface conductance and gas-phase reactions do not play significant roles. While higher in the PBL, mixing is dominantly driven by thermal mixing, induced by the buoyancy of heated and/or moist air near the surface; turbulent mixing in the surface layer is predominantly induced by mechanical shearing, which can be reflected by u_* (Stull, 1988).

Fig. 10 presents the bin-based linear regression slope coefficient (LRSC) and the corresponding r^2 of G_{ns} vs. both u_* and C_{O_3}, while the response to atmospheric stability is presented in Section S6. Fig. 10 clearly indicates no significant correlation between G_{ns} and C_{O_3}. On the contrary, an anticorrelation is evident during most of the measurement periods, for both daytime and nighttime, probably due to the sensitivity of G_{ns} to other factors. For instance, the relatively strong daytime

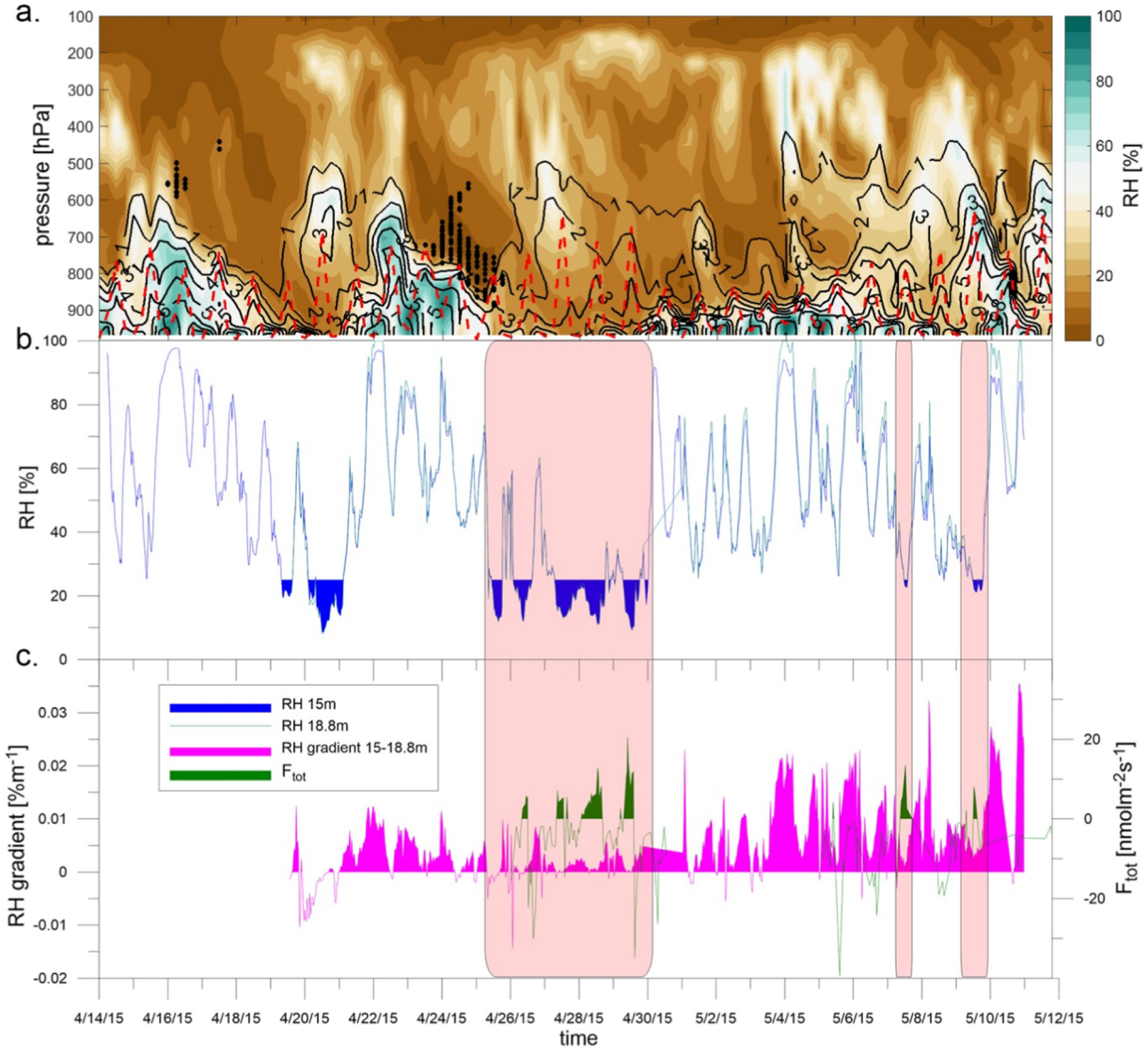

Fig. 9. Positive total O_3 flux (F_{tot}) events induced by extreme dry surface conditions under dry intrusion (DI) events. (a) Vertical profile at 31°N 35°E of relative humidity (RH; shaded, %) and specific humidity (g kg^{-1}, black contours) vs. time from ERA Interim. The black dots mark the time and pressure level of DI trajectories that are present within a 1° distance from 31°N 35°E. The dashed red line marks the PBL height. (b) RH measurements at heights of 15 m and 18.8 m above the surface, with blue-filled area marking RH < 25%. (c) F_{tot} and RH gradient between 15 and 18.8 m. Filled areas represent positive F_{tot} (dark green) and positive RH gradient (magenta), respectively. The shadowed area in panels b and c shows the synchronization between positive F_{tot} and extremely low RH caused by the DI events.

anticorrelation between C_{O_3} and G_{ns} for Has-WIN-15 can be attributed to a positive correlation between G_{ns} and RH, considering that in general, C_{O_3} tends to anticorrelate with RH (see Section 3.4.2). In this study, C_{O_3} was also found to play only a relatively minor role in influencing F_{st} during most of the measurements (Section 3.3), and the results presented in Fig. 10 indicate that F_{ns} is not sensitive to C_{O_3} either, considering the generally small F_{st}/F_{tot} (<50% in all cases) under the studied conditions. A relatively small impact of C_{O_3} on O_3 deposition was indicated based on several studies, including, for instance, investigation of O_3 deposition to a ponderosa pine plantation in Sierra Nevada (Kurpius et al., 2002) or to Norway spruce and cembran pine (Mikkelsen et al., 2000; Wieser et al., 2000).

Fig. 10 indicates a significantly higher association between G_{ns} and u_* during the night vs. daytime. This implies that while during the day, when air mixing is relatively high, O_3 deposition is not significantly limited by air mixing, during the night, higher atmospheric stability results in a higher dependence on air mixing (see Fares et al., 2014; Lamaud et al., 2002; Sun and Massman, 1999).

The relatively high impact of RH on non-stomatal O_3 deposition during the night via surface wetness formation (see Section 3.4.2) requires efficient mixing of the air to facilitate its vertical transport to the wetted surface. Therefore, considering the restricted air mixing at night, dependence of G_{ns} on u_* is expected in the case of G_{ns} dependence on RH. A comparison of Figs. 8 and 10 indeed indicates that, in most cases, ERSC for G_{ns} vs. RH is relatively high, and LRSC for G_{ns} vs. u_* is also relatively high. Exceptional is Esh-SUM-14 for which the extremely high ERSC for G_{ns} vs. RH may not be accurate, because it is based on a small number of bins. The relatively high correlation between G_{ns} dependence on both RH and u_* may further suggest synchronization in the efficiency level of these related processes, considering that both u_* and RH can be increased by sea/land breeze. Previous studies in the Eastern Mediterranean have indicated that a typical scale for the inland effects of sea/land breezes, including increased wind speed and RH, as well as enrichment of transported air masses with marine aerosols, is about 100 km inland from the seashore, starting in the afternoon and lasting several hours (Derimian et al., 2017; Feliks, 1993).

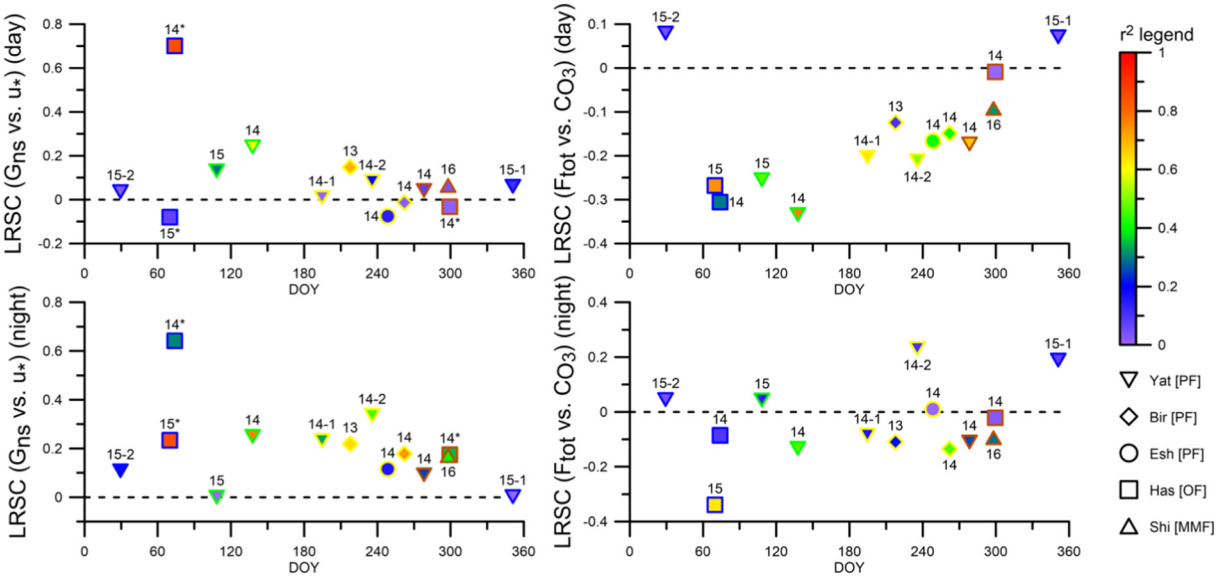

Fig. 10. Response of non-stomatal O_3 conductance (G_{ns}) to friction velocity (u_*) and total O_3 conductance (G_{tot}) to O_3 mixing ratio (C_{O_3}). Presented are the linear regression slope coefficient (LRSC) values for the bin-based exponential regression between G_{ns} vs. u_* (left panels) and F_{tot} vs. C_{O_3} (right panels) during the day (upper panels) and at night (lower panels). Different sites and seasons are represented by different symbols and line colors, respectively, labeled with year (see Tables 1 and 2 for site and measurement period abbreviations). The filling color represents the r^2 value as per the color key on the figure. Dashed line is the zero line of the LRSC. *See Section 2.3 for potential inaccuracies in F_{tot} partitioning.

Our analyses indicated a clear correlation between u_* and wind speed (see Figs. S2 and S3), while wind speed was significantly influenced by sea and land breezes. While during the summer, the sea breeze is generally more intense than the land breeze, in winter, the land breeze is generally more intense. This resulted in a typically more elevated u_* late at night in winter vs. summer, when u_* tended to increase more continuously during the night (see Fig. S2). Note also for Bir-SUM-13, Yat-SUM-14-1 and Bir-SUM-14 where, in most cases, wind was flowing from the west during the whole night (Fig. S3), as was also confirmed by simulation using a trajectory model, HYSPLIT, u_* also showed a significant correlation with wind speed, which gradually decreased during the night (Section S4).

While the sea/land breeze gradually becomes less effective during the night, the sensitivity of G_{ns} to RH and u_* may still be important considering the increasing sensitivity of G_{ns} to u_* under small u_*, together with the smaller impact of other processes on O_3 deposition during the night, such as reaction of O_3 with BVOCs and stomatal O_3 uptake. While several studies on O_3 deposition over different canopy types and seawater have indicated that the response of G_{ns} to changes in u_* becomes significantly smaller for $u_* > 0.2$–0.4 m s^{-1} (Colbeck and Harrison, 1985; Gallagher et al., 2001; Rannik et al., 2009; Zhang et al., 2002), under the studied conditions, a relatively strong dependence of u_* on G_{ns} during the night was also associated with $u_* > 0.4$. For instance, Fig. 10 indicates relatively high LRSC for the nighttime regression of u_* vs. G_{ns} and corresponding r^2 for Bir-SUM-13 and Has-WIN-15, whereas u_* values during these measurements were higher, on average, than 0.4 much of the time (Fig. S2). This may reinforce the notion that the impacts of u_* and RH on G_{ns} tend to be synchronized. Namely, in some cases for which u_* is not a strong limiting factor of G_{ns}, a relatively strong correlation of G_{ns} and u_* is still observed due to high dependence of u_* on RH, during air transport from the sea. The overall relatively strong stimulation of nighttime G_{ns} by u_* and RH can also explain the small V_d-d/V_d-n in autumn and early winter (Section 3.2) compared to the other seasons, considering that both F_{st} and the daytime reaction of O_3 with BVOCs tend to be small during this period.

4. Summary

Here, we studied the deposition of O_3 to vegetation under warm and dry conditions along the ICG in the Eastern Mediterranean, including semiarid, Mediterranean and humid Mediterranean sites, at distances of 20–59 km from the seashore. In agreement with our main working hypothesis, our study indicated fundamentally different features of O_3 deposition to vegetation and its partitioning to F_{st} and F_{ns} along the ICG, and significant coastal effects were observed at all sites.

First, our measurements revealed significantly more severe limitation on F_{st} by drought conditions, compared with previous studies in other Mediterranean areas, with average F_{st}/F_{tot} lower than 50% during all measurements. The analyses further indicated fundamental differences in drought limitation on F_{st} between the semiarid site, Yat, and the Mediterranean and humid Mediterranean sites. While at the other sites, F_{st} was positively correlated with VPD during the summer with a somewhat lower correlation in late summer, in Yat, F_{st} was strongly limited by drought conditions, from spring to early winter (prior to precipitation), reaching a minimum average F_{st}/F_{tot} of 8–11% during the summer. For comparison, F_{st}/F_{tot} averaged 44–47% at Esh and Bir during the summer; in winter, F_{st}/F_{tot} in Yat averaged 15–38%. The calculated annual weighted average F_{st}/F_{tot} in Yat was ~21% (see Section S10). Overall, integrated F_{st} decreased with decreasing precipitation following the order Bir > Esh > Yat, while integrated F_{st} in Yat followed the order winter > spring > summer > autumn/early winter.

While previous studies under Mediterranean conditions revealed the important contribution of chemical reactions, mainly with BVOCs, to O_3 deposition, under the conditions studied here, RH was found to be the most important factor controlling O_3 deposition rate, via enhancement of F_{ns} at all sites. RH seemed to predominantly affect G_{ns} by controlling the formation of surface wetness during the night and day for RH > ~70%. A correlation between RH and G_{ns} for RH < 70%, in some cases, reinforced previous findings about the effect of aerosols in stimulating surface wetness formation, following their deposition on the surface.

Efficient O_3 deposition during the night was associated with relatively high RH and u_*. The high u_* was found to be facilitated by sea and land breezes at night, indicating significant enhancement of O_3 deposition during the night by this effect, dozens of kilometers from the sea. This enhanced nighttime deposition together with the lower daytime RH resulted in V_d-d being only ~8% larger than V_d-n in late autumn and early winter.

To the best of our knowledge, this is the first time that unique phenomenon of positive F_{tot} induced by extreme dry conditions near the

ground has been shown. At least in some cases, the extreme dryness was facilitated by a synoptic-scale DI. Additional study is required to determine the factors controlling the positive F_{tot}, including meteorological conditions and landform types, and its frequency, geographical distribution and potential impact on different spatial scales. Additional research is also required to shed more light on the synoptic-scale meteorological factors controlling the DI event, and the climatological relationship between such synoptic-scale forcing and extreme surface drying conducive to positive F_{tot}.

The contribution of BVOC emission to O_3 deposition was mostly confined to summer and early autumn. Reaction of O_3 with NO had a relatively minor influence on F_{ns}. Our measurements confirmed that NO emission from elevated anthropogenic sources can result in a decrease in F_{tot}, and even positive F_{tot}, which should be taken into account in any study of O_3 flux under anthropogenic NO_X pollution. In agreement with previous studies under Mediterranean conditions, C_{O_3} was found to play no significant role in affecting F_{st} or F_{tot} under the studied conditions, although its effect on F_{st} was somewhat more important in the humid Mediterranean and Mediterranean sites during the summer.

In terms of afforestation management, this study indicates the benefit of establishing forests in semiarid areas, where vegetation can act as a relatively efficient sink for O_3 on a local scale, with only a minimal negative impact on the vegetation. This primarily results from the relatively large F_{ns} fraction and the strong limitation on F_{st}, which result in both low yearly integrated O_3 uptake and generally higher limitation on F_{st} for relatively elevated C_{O_3}. Moreover, subtropical vegetation species have been reported to be much less sensitive than temperate ones (Li et al., 2017). The implications of semiarid forests on photochemistry should be evaluated, but also their impact on regional-scale photochemistry, driven by BVOC emission. Semiarid afforestation has also been found to have a positive effect on ecosystem water yield efficiency (Rohatyn et al., 2018) and precipitation amount (Yosef et al., 2018), but with a negative effect on radiative forcing via reduced albedo (Rotenberg and Yakir, 2010) compared to more temperate areas. Semiarid areas occupy ~18% of the global land surface, and therefore more studies are needed to improve our understanding of the implications on afforestation and desertification in semiarid areas on radiative forcing, also considering the small F_{st}/F_{tot} associated with semiarid forests.

Acknowledgements

This study was supported by the Israel Science Foundation, Grant No.1787/15. E.T. holds the Joseph H. and Belle R. Braun Senior Lectureship in Agriculture.

Appendix A. Supplementary data

Supplementary data to this article can be found online at https://doi.org/10.1016/j.scitotenv.2018.12.272.

References

Abdelkader, M., Metzger, S., Steil, B., Klingmüller, K., Tost, H., Pozzer, A., Stenchikov, G., Barrie, L., Lelieveld, J., 2017. Sensitivity of transatlantic dust transport to chemical aging and related atmospheric processes. Atmos. Chem. Phys. 17 (6), 3799–3821. https://doi.org/10.5194/acp-17-3799-2017.

Ainsworth, E.A., Yendrek, C.R., Sitch, S., Collins, W.J., Emberson, L.D., 2012. The effects of tropospheric ozone on net primary productivity and implications for climate change. Annu. Rev. Plant Biol. 63, 637–661. https://doi.org/10.1146/annurev-arplant-042110-103829.

Alper-Siman, Tov D., Peleg, M., Matveev, V., Mahrer, Y., Seter, I., Luria, M., 1997. Recirculation of polluted air masses over the East Mediterranean coast. Atmos. Environ. 31 (10), 1441–1448. https://doi.org/10.1016/S1352-2310(96)00321-4.

Altimir, N., Tuovinen, J.-P., Vesala, T., Kulmala, M., Hari, P., 2004. Measurements of ozone removal by Scots pine shoots: calibration of a stomatal uptake model including the non-stomatal component. Atmos. Environ. 38 (15), 2387–2398. https://doi.org/10.1016/j.atmosenv.2003.09.077.

Altimir, N., Kolari, P., Tuovinen, J.-P., Vesala, T., Bäck, J., Suni, T., Kulmala, M., Hari, P., 2006. Foliage surface ozone deposition: a role for surface moisture? Biogeosciences 3, 209–228 (https://www.biogeosciences.net/3/209/2006/).

Anav, A., de Marco, A., Proietti, C., Alessandri, A., Dell'Aquila, A., Cionni, I., Friedlingstein, P., Khvorostyanov, D., Menut, L., Paoletti, E., Sicard, P., Sitch, S., Vitale, M., 2016. Comparing concentration-based (AOT40) and stomatal uptake (PODY) metrics for ozone risk assessment to European forests. Glob. Chang. Biol. 22 (4), 1608–1627. https://doi.org/10.1111/gcb.13138.

Anav, A., Liu, Q., de Marco, A., Proietti, C., Savi, F., Paoletti, E., Piao, S., 2018a. The role of plant phenology in stomatal ozone flux modeling. Glob. Chang. Biol. 24 (1), 235–248. https://doi.org/10.1111/gcb.13823.

Anav, A., Proietti, C., Menut, L., Carnicelli, S., Marco, A., de, Paoletti E., 2018b. Sensitivity of stomatal conductance to soil moisture: implications for tropospheric ozone. Atmos. Chem. Phys. 18 (8), 5747–5763. https://doi.org/10.5194/acp-18-5747-2018.

Asaf, D., Rotenberg, E., Tatarinov, F., Dicken, U., Montzka, S.A., Yakir, D., 2013. Ecosystem photosynthesis inferred from measurements of carbonyl sulphide flux. Nat. Geosci. 6 (3), 186–190. https://doi.org/10.1038/ngeo1730.

Ashmore, M.R., 2005. Assessing the future global impacts of ozone on vegetation. Plant Cell Environ. 28 (8), 949–964. https://doi.org/10.1111/j.1365-3040.2005.01341.x.

Aubinet, M., Vesala, T., Papale, D., 2012. Eddy Covariance: A Practical Guide to Measurement and Data Analysis. Springer, Dordrecht, New York.

Bauer, M.R., Hultman, N.E., Panek, J.A., Goldstein, A.H., 2000. Ozone deposition to a ponderosa pine plantation in the Sierra Nevada Mountains (CA): a comparison of two different climatic years. J. Geophys. Res. 105 (D17), 22123–22136.

Becerril-Piña, R., Mastachi-Loza, C.A., González-Sosa, E., Díaz-Delgado, C., Bâ, K.M., 2015. Assessing desertification risk in the semi-arid highlands of central Mexico. J. Arid Environ. 120, 4–13. https://doi.org/10.1016/j.jaridenv.2015.04.006.

Bender, J., Weigel, H.-J., 2011. Changes in atmospheric chemistry and crop health: a review. Agron. Sustain. Dev. 31 (1), 81–89. https://doi.org/10.1051/agro/2010013.

Bouvier-Brown, N.C., Goldstein, A.H., Gilman, J.B., Kuster, W.C., de Gouw, J.A., 2009. In-situ ambient quantification of monoterpenes, sesquiterpenes, and related oxygenated compounds during BEARPEX 2007 – implications for gas- and particle-phase chemistry. Atmos. Chem. Phys. Discuss. 9 (2), 10235–10269. https://doi.org/10.5194/acpd-9-10235-2009.

Browning, K.A., 1997. The dry intrusion perspective of extra-tropical cyclone development. Meteorol. Appl. 4 (4), 317–324. https://doi.org/10.1017/S1350482797000613.

Burkhardt, J., Eiden, R., 1994. Thin water films on coniferous needles: a new device for the study of water vapour condensation and gaseous deposition to plant surfaces and particle samples. Atmos. Environ. 28 (12), 2001–2017.

Caird, M.A., Richards, J.H., Donovan, L.A., 2007. Nighttime stomatal conductance and transpiration in C3 and C4 plants. Plant Physiol. 143 (1), 4–10. https://doi.org/10.1104/pp.106.092940.

Cape, J.N., Hamilton, R., Heal, M.R., 2009. Reactive uptake of ozone at simulated leaf surfaces: implications for 'non-stomatal' ozone flux. Atmos. Environ. 43 (5), 1116–1123. https://doi.org/10.1016/j.atmosenv.2008.11.007.

Chamberlain, A.C., Chadwick, R.C., 1953. Deposition of airborne radioiodine vapor. Health Environ. Res. 8, 22–25.

Chameides, W.L., Stelson, A.W., 1992. Aqueous-phase chemical processes in deliquescent sea-salt aerosols: a mechanism that couples the atmospheric cycles of S and sea salt. J. Geophys. Res. 97 (D18), 20565. https://doi.org/10.1029/92JD01923.

Cieslik, S., 2009. Ozone fluxes over various plant ecosystems in Italy: a review. Environ. Pollut. 157 (5), 1487–1496. https://doi.org/10.1016/j.envpol.2008.09.050.

Colbeck, I., Harrison, R.M., 1985. Dry deposition of ozone: some measurements of deposition velocity and of vertical profiles to 100 metres. Atmos. Environ. 19 (11), 1807–1818.

Dayan, U., Levy, I., 2002. Relationship between synoptic-scale atmospheric circulation and ozone concentrations over Israel. J. Geophys. Res. 107 (D24), 1441. https://doi.org/10.1029/2002JD002147.

Dayan, U., Rodnizki, J., 1999. The temporal behavior of the atmospheric boundary layer in Israel. J. Appl. Meteorol. 38 (6), 830–836. https://doi.org/10.1175/1520-0450(1999)038<0830:TTBOTA>2.0.CO;2.

Dayan, U., Ricaud, P., Zbinden, R., Dulac, F., 2017. Atmospheric pollution concentrations over the Eastern Mediterranean during summer – a review. Atmos. Chem. Phys. Discuss., 1–65 https://doi.org/10.5194/acp-2017-79.

de Marco, A., Sicard, P., Fares, S., Tuovinen, J.-P., Anav, A., Paoletti, E., 2016. Assessing the role of soil water limitation in determining the Phytotoxic Ozone Dose (PODY) thresholds. Atmos. Environ. 147, 88–97. https://doi.org/10.1016/j.atmosenv.2016.09.066.

Dee, D.P., Uppala, S., 2009. Variational bias correction of satellite radiance data in the ERA-Interim reanalysis. Q. J. R. Meteorol. Soc. 135 (644), 1830–1841. https://doi.org/10.1002/qj.493.

Dee, D.P., Uppala, S.M., Simmons, A.J., Berrisford, P., Poli, P., Kobayashi, S., Andrae, U., Balmaseda, M.A., Balsamo, G., Bauer, P., Bechtold, P., Beljaars, A.C.M., van de Berg, L., Bidlot, J., Bormann, N., Delsol, C., Dragani, R., Fuentes, M., Geer, A.J., Haimberger, L., Healy, S.B., Hersbach, H., Hólm, E.V., Isaksen, L., Kållberg, P., Köhler, M., Matricardi, M., McNally, A.P., Monge-Sanz, B.M., Morcrette, J.-J., Park, B.-K., Peubey, C., de Rosnay, P., Tavolato, C., Thépaut, J.-N., Vitart, F., 2011. The ERA-Interim reanalysis: configuration and performance of the data assimilation system. Q. J. R. Meteorol. Soc. 137 (656), 553–597. https://doi.org/10.1002/qj.828.

Derimian, Y., Choël, M., Rudich, Y., Deboudt, K., Dubovik, O., Laskin, A., Legrand, M., Damiri, B., Koren, I., Unga, F., Moreau, M., Andreae, M.O., Karnieli, A., 2017. Effect of sea breeze circulation on aerosol mixing state and radiative properties in a desert setting. Atmos. Chem. Phys. 17 (18), 11331–11353. https://doi.org/10.5194/acp-17-11331-2017.

Dragani, R., 2011. On the quality of the ERA-Interim ozone reanalyses: comparisons with satellite data. Q. J. R. Meteorol. Soc. 137 (658), 1312–1326. https://doi.org/10.1002/qj.821.

ECMWF, 2007. IFS documentation CY31R1—part IV: physical processes. https://www.ecmwf.int/sites/default/files/elibrary/2007/9221-part-iv-physical-processes.pdf.

Emberson, L.D., Wieser, G., Ashmore, M.R., 2000. Modelling of stomatal conductance and ozone ¯ux of Norway spruce: comparison with ®eld data. Environ. Pollut. 109, 393–402.

Emberson, L.D., Büker, P., Ashmore, M.R., 2007. Assessing the risk caused by ground level ozone to European forest trees: a case study in pine, beech and oak across different climate regions. Environ. Pollut. 147 (3), 454–466. https://doi.org/10.1016/j.envpol.2006.10.026.

Fares, S., Mereu, S., Scarascia, Mugnozza G., Vitale, M., Manes, F., Frattoni, M., Ciccioli, P., Gerosa, G., Loreto, F., 2009. The ACCENT-VOCBAS field campaign on biosphere-atmosphere interactions in a Mediterranean ecosystem of Castelporziano (Rome): site characteristics, climatic and meteorological conditions, and eco-physiology of vegetation and eco-physiology of vegetation. Biogeosciences 6, 1043–1058.

Fares, S., Goldstein, A., Loreto, F., 2010a. Determinants of ozone fluxes and metrics for ozone risk assessment in plants. J. Exp. Bot. 61 (3), 629–633. https://doi.org/10.1093/jxb/erp336.

Fares, S., McKay, M., Holzinger, R., Goldstein, A.H., 2010b. Ozone fluxes in a *Pinus ponderosa* ecosystem are dominated by non-stomatal processes: evidence from long-term continuous measurements. Agric. For. Meteorol. 150 (3), 420–431. https://doi.org/10.1016/j.agrformet.2010.01.007.

Fares, S., Weber, R., Park, J.-H., Gentner, D., Karlik, J., Goldstein, A.H., 2012. Ozone deposition to an orange orchard: partitioning between stomatal and non-stomatal sinks. Environ. Pollut. 169, 258–266. https://doi.org/10.1016/j.envpol.2012.01.030.

Fares, S., Vargas, R., Detto, M., Goldstein, A.H., Karlik, J., Paoletti, E., Vitale, M., 2013. Tropospheric ozone reduces carbon assimilation in trees: estimates from analysis of continuous flux measurements. Glob. Chang. Biol. 19 (8), 2427–2443. https://doi.org/10.1111/gcb.12222.

Fares, S., Savi, F., Muller, J., Matteucci, G., Paoletti, E., 2014. Simultaneous measurements of above and below canopy ozone fluxes help partitioning ozone deposition between its various sinks in a Mediterranean Oak Forest. Agric. For. Meteorol. 198-199, 181–191. https://doi.org/10.1016/j.agrformet.2014.08.014.

Farmer, D.K., Cohen, R.C., 2008. Observations of HNO_3, ΣAN, ΣPN and NO_2 fluxes: evidence for rapid HOx chemistry within a pine forest canopy. Atmos. Chem. Phys. 8, 3899–3917.

Farquhar, G.D., Sharkey, T.D., 1982. Stomatal conductance and photosynthesis. Annu. Rev. Plant Physiol. 33 (1), 317–345. https://doi.org/10.1146/annurev.pp.33.060182.001533.

Feliks, Y., 1991. Downwelling along the northeastern coasts of the Eastern Mediterranean. J. Phys. Oceanogr. 21, 511–526.

Feliks, Y., 1993. A numerical model for estimation of the diurnal fluctuation of the inversion height due to a sea breeze. Bound.-Layer Meteorol. 62 (1–4), 151–161.

Finlayson-Pitts, B.J., Pitts, J.N., 2000. Chemistry of the Upper and Lower Atmosphere: Theory, Experiments, and Applications. Academic Press, San Diego.

Fiscuc, E.L., Booker, F.L., Burkey, K.O., 2005. Crop responses to ozone: uptake, modes of action, carbon assimilation and partitioning. Plant Cell Environ. 28, 997–1011.

Foken, T., Wichura, B., 1996. Tools for quality assessment of surface-based flux measurements. Agric. For. Meteorol. 78 (1–2), 83–105. https://doi.org/10.1016/0168-1923(95)02248-1.

Foken, T., Skeib, G., Richter, S.H., 1991. Dependence of the integral turbulence characteristics on the stability of stratification and their use for Doppler-Sodar measurements. Z. Meteorol. 41 (4), 311–315.

Fowler, D., Flechard, C., Cape, J.N., Storeton-West, R.L., Coyle, M., 2001. Measurements of ozone deposition to vegetation quantifying the flux, the stomatal and non-stomatal components. Water Air Soil Pollut. 130 (1–4), 63–74.

Fowler, D., Pilegaard, K., Sutton, M.A., Ambus, P., Raivonen, M., Duyzer, J., Simpson, D., Fagerli, H., Fuzzi, S., Schjoerring, J.K., Granier, C., Neftel, A., Isaksen, I.S.A., Laj, P., Maione, M., Monks, P.S., Burkhardt, J., Daemmgen, U., Neirynck, J., Personne, E., Wichink-Kruit, R., Butterbach-Bahl, K., Flechard, C., Tuovinen, J.P., Coyle, M., Gerosa, G., Loubet, B., Altimir, N., Gruenhage, L., Ammann, C., Cieslik, S., Paoletti, E., Mikkelsen, T.N., Ro-Poulsen, H., Cellier, P., Cape, J.N., Horváth, L., Loreto, F., Niinemets, Ü., Palmer, P.I., Rinne, J., Misztal, P., Nemitz, E., Nilsson, D., Pryor, S., Gallagher, M.W., Vesala, T., Skiba, U., Brüggemann, N., Zechmeister-Boltenstern, S., Williams, J., O'Dowd, C., Facchini, M.C., de Leeuw, G., Flossman, A., Chaumerliac, N., Erisman, J.W., 2009. Atmospheric composition change: ecosystems–atmosphere interactions. Atmos. Environ. 43 (33), 5193–5267. https://doi.org/10.1016/j.atmosenv.2009.07.068.

Fratini, G., Ibrom, A., Arriga, N., Burba, G., Papale, D., 2012. Relative humidity effects on water vapour fluxes measured with closed-path eddy-covariance systems with short sampling lines. Agric. For. Meteorol. 165, 53–63. https://doi.org/10.1016/j.agrformet.2012.05.018.

Gallagher, M.W., Beswick, K.M., Coe, H., 2001. Ozone deposition to coastal waters. Q. J. R. Meteorol. Soc. 127, 539–558.

Ganzeveld, L., Bouwman, L., Stehfest, E., van Vuuren, D.P., Eickhout, B., Lelieveld, J., 2010. Impact of future land use and land cover changes on atmospheric chemistry-climate interactions. J. Geophys. Res. 115 (D23), 3. https://doi.org/10.1029/2010JD014041.

Gerosa, G., Vitale, M., Finco, A., Manes, F., Denti, A., Cieslik, S., 2005. Ozone uptake by an evergreen Mediterranean Forest (*Quercus ilex*) in Italy. Part I: micrometeorological flux measurements and flux partitioning. Atmos. Environ. 39 (18), 3255–3266. https://doi.org/10.1016/j.atmosenv.2005.01.056.

Gerosa, G., Finco, A., Mereu, S., Vitale, M., Manes, F., Denti, A.B., 2009. Comparison of seasonal variations of ozone exposure and fluxes in a Mediterranean Holm oak forest between the exceptionally dry 2003 and the following year. Environ. Pollut. 157 (5), 1737–1744. https://doi.org/10.1016/j.envpol.2007.11.025.

Goldstein, A.H., McKay, M., Kurpius, M.R., Schade, G.W., Lee, A., Holzinger, R., Rasmussen, R.A., 2004. Forest thinning experiment confirms ozone deposition to forest canopy is dominated by reaction with biogenic VOCs. Geophys. Res. Lett. 31 (22), 22,123. https://doi.org/10.1029/2004GL021259.

Guenther, A.B., Zimmerman, P.R., Harley, P.C., Monson, R.K., Fall, R., 1993. Isoprene and monoterpene emission rate variability model evaluations and sensitivity analyses. J. Geophys. Res. 98 (D7), 12609–12617.

Gupta, D., Eom, H.-J., Cho, H.-R., Ro, C.-U., 2015. Hygroscopic behavior of NaCl–$MgCl_2$ mixture particles as nascent sea-spray aerosol surrogates and observation of efflorescence during humidification. Atmos. Chem. Phys. 15 (19), 11273–11290. https://doi.org/10.5194/acp-15-11273-2015.

Hardacre, C., Wild, O., Emberson, L., 2015. An evaluation of ozone dry deposition in global scale chemistry climate models. Atmos. Chem. Phys. 15 (11), 6419–6436. https://doi.org/10.5194/acp-15-6419-2015.

Hersey, S.P., Sorooshian, A., Murphy, S.M., Flagan, R.C., Seinfeld, J.H., 2009. Aerosol hygroscopicity in the marine atmosphere: a closure study using high-time-resolution, multiple-RH DASH-SP and size-resolved C-ToF-AMS data. Atmos. Chem. Phys. 9, 2543–2554.

Holzinger, R., Lee, A., Paw, K.T., Goldstein, U.A.H., 2005. Observations of oxidation products above a forest imply biogenic emissions of very reactive compounds. Atmos. Chem. Phys. 5 (1), 67–75. https://doi.org/10.5194/acp-5-67-2005.

Jacob, D., 2000. Heterogeneous chemistry and tropospheric ozone. Atmos. Environ. 34 (12–14), 2131–2159. https://doi.org/10.1016/S1352-2310(99)00462-8.

Keene, W.C., 2002. Variation of marine aerosol acidity with particle size. Geophys. Res. Lett. 29 (7), 20,565. https://doi.org/10.1029/2001GL013881.

Keene, W.C., Savoie, D.L., 1998. The pH of deliquesced sea-salt aerosol in polluted marine air. Geophys. Res. Lett. 25 (12), 2181–2184. https://doi.org/10.1029/98GL01591.

Kley, D., Kleinmann, M., Sanderman, H., Krupa, S., 1999. Photochemical oxidants: state of the science. Environ. Pollut. 100 (1–3), 19–42.

Kurpius, M.R., Goldstein, A.H., 2003. Gas-phase chemistry dominates O_3 loss to a forest, implying a source of aerosols and hydroxyl radicals to the atmosphere. Geophys. Res. Lett. 30 (7), 121. https://doi.org/10.1029/2002GL016785.

Kurpius, M.R., McKay, M., Goldstein, A.H., 2002. Annual ozone deposition to a Sierra Nevada ponderosa pine plantation. Atmos. Environ. 36 (28), 4503–4515. https://doi.org/10.1016/S1352-2310(02)00423-5.

Laisk, A., Kull, O., Moldau, H., 1989. Ozone concentration in leaf intercellular air spaces is close to zero. Plant Physiol. 90 (3), 1163–1167. https://doi.org/10.1104/pp.90.3.1163.

Lal, R., 2004. Carbon sequestration in dryland ecosystems. Environ. Manag. 33 (4), 528–544. https://doi.org/10.1007/s00267-003-9110-9.

Lamaud, E., Carrara, A., Brunet, Y., Lopez, A., Druilhet, A., 2002. Ozone fluxes above and within a pine forest canopy in dry and wet conditions. Atmos. Environ. 36 (1), 77–88. https://doi.org/10.1016/S1352-2310(01)00468-X.

Lamaud, E., Loubet, B., Irvine, M., Stella, P., Personne, E., Cellier, P., 2009. Partitioning of ozone deposition over a developed maize crop between stomatal and non-stomatal uptakes, using eddy-covariance flux measurements and modelling. Agric. For. Meteorol. 149 (9), 1385–1396. https://doi.org/10.1016/j.agrformet.2009.03.017.

Launiainen, S., Katul, G.G., Grönholm, T., Vesala, T., 2013. Partitioning ozone fluxes between canopy and forest floor by measurements and a multi-layer model. Agric. For. Meteorol. 173, 85–99. https://doi.org/10.1016/j.agrformet.2012.12.009.

Lelieveld, J., Dentener, F.J., 2000. What controls tropospheric ozone? J. Geophys. Res. 105 (D3), 3531–3551. https://doi.org/10.1029/1999JD901011.

Li, P., Feng, Z., Catalayud, V., Yuan, X., Xu, Y., Paoletti, E., 2017. A meta-analysis on growth, physiological, and biochemical responses of woody species to ground-level ozone highlights the role of plant functional types. Plant Cell Environ. 40 (10), 2369–2380. https://doi.org/10.1111/pce.13043.

Li, P., de Marco, A., Feng, Z., Anav, A., Zhou, D., Paoletti, E., 2018. Nationwide ground-level ozone measurements in China suggest serious risks to forests. Environ. Pollut. 237, 803–813. https://doi.org/10.1016/j.envpol.2017.11.002.

Li, Q., Gabay, M., Rubin, Y., Fredj, E., Tas, E., 2018. Measurement-based investigation of ozone deposition to vegetation under the effects of coastal and photochemical air pollution in the Eastern Mediterranean. Sci. Total Environ. 645, 1579–1597. https://doi.org/10.1016/j.scitotenv.2018.07.037.

Llusia, J., Roahtyn, S., Yakir, D., Rotenberg, E., Seco, R., Guenther, A., Peñuelas, J., 2016. Photosynthesis, stomatal conductance and terpene emission response to water availability in dry and mesic Mediterranean forests. Trees 30 (3), 749–759. https://doi.org/10.1007/s00468-015-1317-x.

Lombardozzi, D., Sparks, J.P., Bonan, G., Levis, S., 2012. Ozone exposure causes a decoupling of conductance and photosynthesis: implications for the Ball-Berry stomatal conductance model. Oecologia 169 (3), 651–659. https://doi.org/10.1007/s00442-011-2242-3.

Lombardozzi, D., Sparks, J.P., Bonan, G., 2013. Integrating O_3; influences on terrestrial processes: photosynthetic and stomatal response data available for regional and global modeling. Biogeosciences 10 (11), 6815–6831. https://doi.org/10.5194/bg-10-6815-2013.

Lombardozzi, D., Levis, S., Bonan, G., Hess, P.G., Sparks, J.P., 2015. The influence of chronic ozone exposure on global carbon and water cycles. J. Clim. 28 (1), 292–305. https://doi.org/10.1175/JCLI-D-14-00223.1.

Loreto, F., Schnitzler, J.-P., 2010. Abiotic stresses and induced BVOCs. Trends Plant Sci. 15 (3), 154–166. https://doi.org/10.1016/j.tplants.2009.12.006.

Maier-Maercker, U., Koch, W., 1991. Experiments on the control capacity of stomata of *Picea abies* (L.) Karst. after fumigation with ozone and in environmentally damaged material. Plant Cell Environ. 14, 175–184.

Massman, W.J., 2004. Toward an ozone standard to protect vegetation based on effective dose: a review of deposition resistances and a possible metric. Atmos. Environ. 38 (15), 2323–2337. https://doi.org/10.1016/j.atmosenv.2003.09.079.

Matyssek, R., Bytnerowicz, A., Karlsson, P.-E., Paoletti, E., Sanz, M., Schaub, M., Wieser, G., 2007. Promoting the O_3 flux concept for European forest trees. Environ. Pollut. 146 (3), 587–607. https://doi.org/10.1016/j.envpol.2006.11.011.

Meixner, F.X., Yang, W.X., 2006. Biogenic emissions of nitric oxide and nitrous oxide from arid and semi-arid land. In: D'Odorico, P., Porporato, A. (Eds.), Dryland Ecohydrology. Kluwer Academic Publishers, Dordrecht, pp. 233–255.

Metzger, S., Lelieveld, J., 2007. Reformulating atmospheric aerosol thermodynamics and hygroscopic growth into fog, haze and clouds. Atmos. Chem. Phys. 7 (12), 3163–3193. https://doi.org/10.5194/acp-7-3163-2007.

Michou, M., Laville, P., Serça, D., Fotiadi, A., Bouchou, P., Peuch, V.-H., 2005. Measured and modeled dry deposition velocities over the ESCOMPTE area. Atmos. Res. 74 (1–4), 89–116. https://doi.org/10.1016/j.atmosres.2004.04.011.

Mikkelsen, T.N., Ro-Poulsen, H., Pilegaard, K., Hovmand, M.F., Jensen, N.O., Christensen, C.S., Hummelshoej, P., 2000. Ozone uptake by an evergreen forest canopy: temporal variation and possible mechanisms. Environ. Pollut. 109, 423–429.

Moncrieff, J.B., Massheder, J.M., de Bruin, H., Elbers, J., Friborg, T., Heusinkveld, B., Kabat, P., Scott, S., Soegaard, H., Verhoef, A., 1997. A system to measure surface fluxes of momentum, sensible heat, water vapour and carbon dioxide. J. Hydrol. 188-189, 589–611. https://doi.org/10.1016/S0022-1694(96)03194-0.

Monteith, J.L., 1981. Evaporation and surface temperature. Q. J. R. Meteorol. Soc. 107, 1–27.

Niinemets, U., Loreto, F., Reichstein, M., 2004. Physiological and physicochemical controls on foliar volatile organic compound emissions. Trends Plant Sci. 9 (4), 180–186. https://doi.org/10.1016/j.tplants.2004.02.006.

Owen, S., Boissard, C., Street, R.A., Duckham, S.C., Csiky, O., Hewitt, C.N., 1997. Screening of 18 Mediterranean plant species for volatile organic compound emissions. Atmos. Environ. 31, 101–117. https://doi.org/10.1016/S1352-2310(97)00078-2.

Panek, J.A., 2004. Ozone uptake, water loss and carbon exchange dynamics in annually drought-stressed *Pinus ponderosa* forests: measured trends and parameters for uptake modeling. Tree Physiol. 24, 277–290.

Paoletti, E., 2005. Ozone slows stomatal response to light and leaf wounding in a Mediterranean evergreen broadleaf, *Arbutus unedo*. Environ. Pollut. 134 (3), 439–445. https://doi.org/10.1016/j.envpol.2004.09.011.

Paoletti, E., Grulke, N.E., 2005. Does living in elevated CO_2 ameliorate tree response to ozone? A review on stomatal responses. Environ. Pollut. 137 (3), 483–493. https://doi.org/10.1016/j.envpol.2005.01.035.

Pearson, M., Mansfield, T.A., 1993. Interacting effects of ozone and water stress on the stomatal resistance of beech (*Fagus sylvatica* L.). New Phytol. 123 (2), 351–358. https://doi.org/10.1111/j.1469-8137.1993.tb03745.x.

Pszenny, A.A.P., Moldanová, J., Keene, W.C., Sander, R., Maben, J.R., Martinez, M., Crutzen, P.J., Perner, D., Prinn, R.G., 2004. Halogen cycling and aerosol pH in the Hawaiian marine boundary layer. Atmos. Chem. Phys. 4 (1), 147–168. https://doi.org/10.5194/acp-4-147-2004.

Rannik, Ü., Mammarella, I., Keronen, P., Vesala, T., 2009. Vertical advection and nocturnal deposition of ozone over a boreal pine forest. Atmos. Chem. Phys. 9 (6), 2089–2095. https://doi.org/10.5194/acp-9-2089-2009.

Raveh-Rubin, S., 2017. Dry intrusions: Lagrangian climatology and dynamical impact on the planetary boundary layer. J. Clim. 30 (17), 6661–6682. https://doi.org/10.1175/JCLI-D-16-0782.1.

Raveh-Rubin, S., Wernli, H., 2016. Large-scale wind and precipitation extremes in the Mediterranean: dynamical aspects of five selected cyclone events. Q. J. R. Meteorol. Soc. 142 (701), 3097–3114. https://doi.org/10.1002/qj.2891.

Reynolds, O., 1894. On the dynamical theory of incompressible viscous fluids and the determination of the criterion. Phil. Trans. R. Soc. A 186, 123–164.

Richards, N.A.D., Arnold, S.R., Chipperfield, M.P., Miles, G., Rap, A., Siddans, R., Monks, S.A., Hollaway, M.J., 2013. The Mediterranean summertime ozone maximum: global emission sensitivities and radiative impacts. Atmos. Chem. Phys. 13 (5), 2331–2345. https://doi.org/10.5194/acp-13-2331-2013.

Rohatyn, S., Rotenberg, E., Ramati, E., Tatarinov, F., Tas, E., Yakir, D., 2018. Differential impacts of land use and precipitation on 'ecosystem water yield'. Water Resour. Res. https://doi.org/10.1029/2017WR022267.

Rotenberg, E., Yakir, D., 2010. Contribution of semi-arid forests to the climate system. Science (New York, N.Y.) 327 (5964), 451–454. https://doi.org/10.1126/science.1180871.

Rydsaa, J.H., Stordal, F., Gerosa, G., Finco, A., Hodnebrog, Ø., 2016. Evaluating stomatal ozone fluxes in WRF-Chem: comparing ozone uptake in Mediterranean ecosystems. Atmos. Environ. 143, 237–248. https://doi.org/10.1016/j.atmosenv.2016.08.057.

Seco, R., Karl, T., Turnipseed, A., Greenberg, J., Guenther, A., Llusia, J., Peñuelas, J., Dicken, U., Rotenberg, E., Kim, S., Yakir, D., 2017. Springtime ecosystem-scale monoterpene fluxes from Mediterranean pine forests across a precipitation gradient. Agric. For. Meteorol. 237-238, 150–159. https://doi.org/10.1016/j.agrformet.2017.02.007.

Silva, S.J., Heald, C.L., 2018. Investigating dry deposition of ozone to vegetation. J. Geophys. Res. Atmos. 123 (1), 559–573. https://doi.org/10.1002/2017JD027278.

Sitch, S., Cox, P.M., Collins, W.J., Huntingford, C., 2007. Indirect radiative forcing of climate change through ozone effects on the land-carbon sink. Nature 448 (7155), 791–794. https://doi.org/10.1038/nature06059.

Sprenger, M., Wernli, H., 2015. The LAGRANTO Lagrangian analysis tool – version 2.0. Geosci. Model Dev. 8 (8), 2569–2586. https://doi.org/10.5194/gmd-8-2569-2015.

Staudt, M., Seufert, G., 1995. Light-dependent emission of monoterpenes by holm oak (*Quercus ilex* L.). Naturwissenschaften 82 (2), 89–92. https://doi.org/10.1007/BF01140148.

Stella, P., Personne, E., Loubet, B., Lamaud, E., Ceschia, E., Béziat, P., Bonnefond, J.M., Irvine, M., Keravec, P., Mascher, N., Cellier, P., 2011. Predicting and partitioning ozone fluxes to maize crops from sowing to harvest: the Surfatm-O_3 model. Biogeosciences 8 (10), 2869–2886. https://doi.org/10.5194/bg-8-2869-2011.

Stull, R.B., 1988. An Introduction to Boundary Layer Meteorology. Kluwer Academic Publishers, Dordrecht, Boston.

Sun, J., Massman, W., 1999. Ozone transport during the California ozone deposition experiment. J. Geophys. Res. 104 (D10), 11939–11948. https://doi.org/10.1029/1999JD900099.

Sun, G.E., McLaughlin, S.B., Porter, J.H., Uddling, J., Mulholland, P.J., Adams, M.B., Pederson, N., 2012. Interactive influences of ozone and climate on streamflow of forested watersheds. Glob. Chang. Biol. 18 (11), 3395–3409. https://doi.org/10.1111/j.1365-2486.2012.02787.x.

Szeicz, G., Long, I.F., 1969. Surface resistance of crop canopies. Water Resour. Res. 5 (3), 622–633.

Tang, I.N., Tridico, A.C., Fung, K.H., 1997. Thermodynamic and optical properties of sea salt aerosols. J. Geophys. Res. 102 (D19), 23269–23275. https://doi.org/10.1029/97JD01806.

Tjoelker, M.G., Volin, J.C., Oleksyn, J., Reich, P.B., 1995. Interaction of ozone pollution and light effects on photosynthesis in a forest canopy experiment. Plant Cell Environ. 18 (8), 895–905. https://doi.org/10.1111/j.1365-3040.1995.tb00598.x.

Val Martin, M., Heald, C.L., Arnold, S.R., 2014. Coupling dry deposition to vegetation phenology in the Community Earth System Model: implications for the simulation of surface O_3. Geophys. Res. Lett. 41 (8), 2988–2996. https://doi.org/10.1002/2014GL059651.

van Dingenen, R., Dentener, F.J., Raes, F., Krol, M.C., Emberson, L., Cofala, J., 2009. The global impact of ozone on agricultural crop yields under current and future air quality legislation. Atmos. Environ. 43 (3), 604–618. https://doi.org/10.1016/j.atmosenv.2008.10.033.

Vickers, D., Mahrt, L., 1997. Quality control and flux sampling problems for tower and aircraft data. J. Atmos. Ocean. Technol. 14 (3), 512–526. https://doi.org/10.1175/1520-0426(1997)014<0512:QCAFSP>2.0.CO;2.

Wernli, H., 1997. A lagrangian-based analysis of extratropical cyclones. II: a detailed case-study. Q. J. R. Meteorol. Soc. 123, 1677–1706.

Wesely, M., Hicks, B.B., 2000. A review of the current status of knowledge on dry deposition. Atmos. Environ. 34 (12–14), 2261–2282. https://doi.org/10.1016/S1352-2310(99)00467-7.

WHO, 2006. WHO Air Quality Guidelines for Particulate Matter, Ozone, Nitrogen Dioxide and Sulfur Dioxide: Global Update 2005, Summary of Risk Assessment. WHO Press, Geneva.

Wieser, G., Häsler, R., Götz, B., Koch, W., Havranek, W.M., 2000. Role of climate, crown position, tree age and altitude in calculated ozone flux into needles of *Picea abies* and *Pinus cembra*: a synthesis. Environ. Pollut. 109, 415–422.

Wild, O., 2007. Modelling the global tropospheric ozone budget: exploring the variability in current models. Atmos. Chem. Phys. 7, 2643–2660.

Wildt, J., Kley, D., Rockel, A., Rockel, P., Segschneider, H.J., 1997. Emission of NO from several higher plant species. J. Geophys. Res. 102 (D5), 5919–5927. https://doi.org/10.1029/96JD02968.

Wilkinson, S., Davies, W.J., 2009. Ozone suppresses soil drying- and abscisic acid (ABA)-induced stomatal closure via an ethylene-dependent mechanism. Plant Cell Environ. 32 (8), 949–959. https://doi.org/10.1111/j.1365-3040.2009.01970.x.

Williams, E.J., Hutchinson, G.L., Fehsenfeld, F.C., 1992. NOx and N_2O emissions from soil. Glob. Biogeochem. Cycles 6 (4), 351–388.

Wittig, V.E., Ainsworth, E.A., Long, S.P., 2007. To what extent do current and projected increases in surface ozone affect photosynthesis and stomatal conductance of trees? A meta-analytic review of the last 3 decades of experiments. Plant Cell Environ. 30 (9), 1150–1162. https://doi.org/10.1111/j.1365-3040.2007.01717.x.

Wolfe, G.M., Thornton, J.A., McKay, M., Goldstein, A.H., 2011. Forest-atmosphere exchange of ozone: sensitivity to very reactive biogenic VOC emissions and implications for in-canopy photochemistry. Atmos. Chem. Phys. 11 (15), 7875–7891. https://doi.org/10.5194/acp-11-7875-2011.

Yosef, G., Walko, R., Avisar, R., Tatarinov, F., Rotenberg, E., Yakir, D., 2018. Large-scale semi-arid afforestation can enhance precipitation and carbon sequestration potential. Sci. Rep. 8 (1), 996. https://doi.org/10.1038/s41598-018-19265-6.

Zhang, L., Brook, J.R., Vet, R., 2002. On ozone dry deposition—with emphasis on non-stomatal uptake and wet canopies. Atmos. Environ. 36 (30), 4787–4799. https://doi.org/10.1016/S1352-2310(02)00567-8.

Zieger, P., Väisänen, O., Corbin, J.C., Partridge, D.G., Bastelberger, S., Mousavi-Fard, M., Rosati, B., Gysel, M., Krieger, U.K., Leck, C., Nenes, A., Riipinen, I., Virtanen, A., Salter, M.E., 2017. Revising the hygroscopicity of inorganic sea salt particles. Nat. Commun. 8, 15883. https://doi.org/10.1038/ncomms15883.